

**CFD assessment of RANS model for simulation of fast mixing nozzle and
coaxial flow using OpenFOAM**

By

Afiq Bin Mohd Laziz

Dissertation submitted in partial fulfilment of
the requirements for the
Bachelor of Engineering (Hons)
(Chemical Engineering)

JANUARY 2010

Universiti Teknologi PETRONAS
Bandar Seri Iskandar
31750 Tronoh
Perak Darul Ridzuan

CERTIFICATION OF APPROVAL

**CFD assessment of RANS model for simulation of fast mixing nozzle and
coaxial flow using OpenFOAM**

by

Afiq Bin Mohd Laziz

A project dissertation submitted to the
Chemical Engineering Programme
Universiti Teknologi PETRONAS
in partial fulfilment of the requirement for the
BACHELOR OF ENGINEERING (Hons)
(CHEMICAL ENGINEERING)

Approved by,

(Dr Ku Zilati Bt Ku Shaari)

UNIVERSITI TEKNOLOGI PETRONAS
TRONOH, PERAK

January 2010

CERTIFICATION OF ORIGINALITY

This is to certify that I am responsible for the work submitted in this project, that the original work is my own except as specified in the references and acknowledgements, and that the original work contained herein have not been undertaken or done by unspecified sources or persons.

AFIQ BIN MOHD LAZIZ

ABSTRACT

The Reynolds Averaged Navier Stokes Equation (RANS) model was applied to describe the turbulent flow in a millimeter channels by cross-flow impingement and also coaxial flow in a jet mixer. The effects of turbulent models in the CFD turbulent flow is studied to help the engineers and researchers in deciding the selection of turbulent model need to be use in order to save the simulation time and also to reduce the errors produced in their simulations. Good agreement of the CFD prediction with the experimental data in certain locations was obtained with the factor of species transport and velocity profile, where dependence of turbulent models and grid sizes were discussed in details. The results show that, the need of grid study is crucial to obtain reliable results with optimum consumption of computer power. SST $k - \epsilon$ and Launder Gibson RSTM models give superior results compare to the other models which both have their own area of applicability. Launder Gibson RSTM model has the capability to predict the flow with the presence of recirculation and vortices, while SST $k - \epsilon$ model favors more for the flow with less recirculation and high velocity. RANS model is incapable to reproduce the vortices structure in the pipe and nozzle but it capable in predicting the area of mixing and the velocity profile correctly in certain locations.

ACKNOWLEDGEMENT

The author wishes to take the opportunity to express his utmost gratitude to the individual that have taken the time and effort to assist the author in completing the project. Without the cooperation of these individuals, no doubt the author would have faced some minor complications throughout the course.

First and foremost the author's utmost gratitude goes to the author's supervisor, Dr Ku Zilati Ku Shaari. Without her guidance and patience, the author would not be succeeded to complete the project. The author has benefited a lot from her advice, guidance, motivation and support from her throughout the thesis period.

Not to forget, sincere regards are dedicated to the author's Internship supervisor, Dr.-Ing. Kerstin Heinen, from BASF Germany; who are willingly to share her expertise and knowledge with the author in order to make a good thesis.

To the Final Year Research Project Coordinator, Mr Tazli Azizan and Dr Khalik for provide him with all the initial information required to begin the project.

To all individuals that has helped the author in any way, but whose name is not mentioned here, the author thank you all for the wonderful supports.

TABLE OF CONTENT

CERTIFICATION OF APPROVAL	i
CERTIFICATION OF ORIGINALITY	ii
ABSTRACT	iii
ACKNOWLEDGEMENT	iv
TABLE OF CONTENT	v
LIST OF FIGURES	vii
LIST OF TABLES	viii
ABBREVIATIONS AND NOMENCLATURES	ix
CHAPTER 1: INTRODUCTION	1
1.1 Background of study	1
1.2 Problem Statement	2
1.3 Objectives and scope of study.....	3
CHAPTER 2: LITERATURE REVIEW	4
2.1 Theory on micro-mixing model	4
2.2 Application of turbulent mixing.....	6
CHAPTER 3: METHODOLOGY	12
3.1 Pre-Processing.....	13
3.2 Running / Solving	14
3.3 Post-Processing	16
3.4 Simulation Setup for Coaxial Flow Case	17
CHAPTER 4: RESULTS AND DISCUSSION	19
4.1 Convergence Check	19
4.2 Grid sensitivity study	21
4.3 Coaxial Flow Jet Mixer	28
CHAPTER 5: CONCLUSION	33

REFERENCES	35
APPENDIX A: Geometry Description for Fast Mixing Nozzle	39
APPENDIX B: Geometry Description for Coaxial Mixer Jet	54
APPENDIX C: Case Setup	73
APPENDIX D: Post-Processing	76

LIST OF FIGURES

Figure 2-1: Concentration field of a passive scalar inside a T-junction	6
Figure 2-2: Sketch of a jet mixer [Tkatchenko, 2006]	8
Figure 3-1: Overall structure of OpenFOAM	12
Figure 3-2: (a) Experiment schematic of the mini-scale jet mixer, (b) Simulation domain geometry	13
Figure 3-3: Example of grid size (in the picture-coarse mesh)	14
Figure 3-4: The 3D domain structure (left) and the mesh grading of the inlet nozzle (right)	18
Figure 4-1: Location of sample point for observation of the convergence	20
Figure 4-2: Location of line plot with velocity magnitude parameter (a) along x-plane and (b) along y-plane	21
Figure 4-3: Line plot of different meshes at parameter turbulent kinetics energy, k (a) along x-direction; (b) along y-direction	23
Figure 4-4: Comparison of contour plot between experimental [Zhe Liu, 2009] with the simulation result at mesh 0.25 and mesh 3	24
Figure 4-5: Line plot of different meshes at the tracer concentration of species B (a) along x-direction; (b) along y-direction	25
Figure 4-6: Line plot of different meshes at the tracer concentration of species B compared with the experimental data	25
Figure 4-7: Trend result of Y-shape nozzle from Peicheng Luo 2007	26
Figure 4-9: Sample line location along the mixer axis	29
Figure 4-10: The distribution of the mean value of the mixture fraction along the mixer axis R-mode (right) and J-mode (left). f_{max} is the maximal mean mixture fraction in the first cross section $xD = 0$ and f_0 is the maximal mean mixture fraction on the mixture centreline in the cross section xD	29
Figure 4-11: Sample line location along radial mixer axis	30
Figure 4-12: The mean profile of the mixture fraction. R-mode: Section (a), (b) and (c). J-mode: Section (d), (e) and (f). f_0 is the maximal mean mixture fraction on the mixture centreline in the cross section xD	30

Figure 4-13: The mean profile of the axial component of velocity. R-mode: Section (a), (b) and (c). J-mode: Section (d), (e) and (f). u_0 is the maximal axial velocity on the mixture centreline in the cross section xD 32

LIST OF TABLES

Table 3-1: Operating conditions from experiment.....15
 Table 3-2: The flow conditions adopted in the simulation18
 Table 4-1: List of meshes22
 Table 4-2: Simulation results for r-mode and j-mode with respect to magnitude velocity and mixture fraction.28

ABBREVIATIONS AND NOMENCLATURES

Symbols

k	Turbulent kinetic energy (specific)	m^2s^{-2}
p	Pressure	N m^{-2}
R	Reynolds stress tensor (specific)	m^2s^{-2}
Re	Reynolds number	-
Re_t	Turbulent Reynolds number	-
t	Time	s
u_i	Component: i of the velocity	m s^{-1}
\bar{u}_i	Averaged velocity component (ensemble averaged)	m s^{-1}
u'_i	Fluctuating part of the velocity component	m s^{-1}
u_*	Friction velocity	m s^{-1}
x_i	Component: i, of the Cartesian coordinates	m
ρ	Density	kg m^{-3}
ε	Dissipation rate of turbulent kinetic energy (specific)	m^2s^{-3}
ω	Specific dissipation rate of turbulent kinetic energy (specific)	s^{-1}
μ	Dynamic viscosity	$\text{N m}^{-2}\text{s}$
ν	Kinematic viscosity	m^2s^{-1}

Abbreviations

CFD	Computational Fluid Dynamics
OPENFOAM	Open Field Operation and Manipulation
LES	Large eddy simulation
RANS	Reynolds Averaged Navier Stokes
RSTM	Reynolds Stress Tensor Model
SST	Shear Stress Tensor
LIF	Laser-induced Fluorescence
LDA	Laser Doppler Anemometry

CHAPTER 1: INTRODUCTION

1.1 Background of study

The chemical processes with fast parallel-competing or consecutive-competing reactions are often encountered in industry, such as the manufacture of fine chemicals, pharmaceuticals, polymers and so on (Baldyga, 1999). The initial mixing of the reactant has a significant impact on the yields and selectivity of the products when the mixing rate of reactants is less than or similar to the chemical reaction rate (Bourne, 2003; Paul, 2003).

As a principal process mixing usually has a significant effect on the performance of chemical reactor (B.G. Lakatos, 2008) because chemical reactions always occur together with the process of different reactive materials contacting each other. Baldyga and Bourne (1999) stated that in their book, mixing is carried out in order to achieve homogenization, which is distributing one material in another to get uniform properties. Turbulent mixing which is also known as turbulent diffusion is referring to mix of fluids by the act of turbulent, accomplished by diffusion. The relationship between mixing and reaction depends on the relative magnitude of the mixing time scale and the reaction time scale. The time scale and the non-uniformity in the space of the mixing process can lead to significant variance in reaction progress.

Traditionally, many of such processes have relied on the stirred tanks operated in a batch or continuous mode (Nere, N.K., 2003). Since a particularly effective mixing of liquids can be hardly achieved in milliseconds in stirred tanks, energy cost can rather be high for the intense mechanical stirring and the addition of large amount of inert solvents, which imposes extra task for the following separation units. Meanwhile, the liquid mixing and the reactions are also uncertain when scaling from the laboratory to pilot to full scale, resulting in loss of product quality and productivity (Paul, 2003).

In the cases where reactions take place at the time scales of millisecond(s) or even faster, the process imposes great challenge to the design of the fast mixing equipment, where the initial mixing is expected to complete in shorter times, e.g. milliseconds or even sub milliseconds. Therefore, control of the mixing process is often the key technology in process engineering for a wide class of products (F.Schwertfirm, 2007). From the experiment of Satoshi Someya (2009), the basic characteristics of the reactive mixing flow of two streams were investigated, and it is found that, over certain range of Re number, mixing and the development of turbulence were remarkably suppressed in the case where there was a chemical reaction.

Mixing, particularly mixing in co-flows has been a subject of investigations for long time because of their practical applications in many engineering devices such as combustion chambers, injection systems, etc. [Egon 2005]. Current studies of the mixing in confined coaxial jets have received considerable attention because the jet interaction causes a great number of physical phenomena to appear. Among them is intermittence at the boundaries of mixing layers that originates due to generation, coalescence, and decay of unsteady vortex structures. [Valery 2006]

1.2 Problem Statement

In chemical reaction systems with fast reactions, continuous mixing and reaction devices like nozzles are used. One typical field of application for mixing nozzles in chemical processes is for liquid precipitation reactions. Numerical flow simulations may be used to predict the mixing behaviour and pressure loss of the mixing nozzle. So, local mixing quality may be investigated under different flow conditions (volumetric flow rates, geometry changes, etc.). Mixing nozzles are typically operated in the turbulent flow regime to assure fast mixing conditions.

Numerical flow simulations of liquid turbulent flows inside mixing nozzles in industrial scale are still mostly done with Reynolds-Averaged-Navier-Stokes (RANS) turbulence models. They do not resolve all scales of the turbulent vortex structures but provide useful results with feasible amount of computational power.

Inside the research project TEP166 “Modelling of mixing and reactions inside nozzles” available modelling methods for simulation of liquid, turbulent reacting flows are investigated. One major goal of this project is the quantification of accuracy of numerical results, concerning influence of turbulence model, influence of numerical grid and micro-mixing model. Therefore different kinds of flows are investigated numerically and model and parameter studies are made. Different turbulent models are investigated and validated with experimental data.

1.3 Objectives and scope of study

Recent advances in numerical simulations, such as computational fluid dynamics (CFD) techniques, have been recognised as an alternative to detailed experimental investigation and traditional mathematical modelling. Simulation of mixing processes in complex domains at high Reynolds numbers is an important engineering problem. Today calculations based on Reynolds averaged Navier-Stokes equations (RANS) are common practice in industry. The rising computational power and the improved numerical techniques are able to resolve more scales presented in turbulent flow. CFD has been demonstrated to be a powerful tool for modelling a mixing process and reactive mixing (for example in Middleton, 1986 and Brucota, 2002) and in Pei-cheng Luo 2007 and Igor Tkatchenko 2006. The goal of this work was to compare the influence of different turbulence models (two-equation and Reynold stress tensor models) and numerical grid on the two cases of fast mixing nozzle and coaxial flow. Validation of these RANS models has been referred to the experimental data from Zhe Liu 2009 and Igor Tkatchenko 2006. The detailed area of their applicability will be investigated. With the quantification of model influence on predicted results, a better evaluation of numerical results is possible. The simulation will be using an open-source CFD tools called OpenFOAM.

CHAPTER 2: LITERATURE REVIEW

2.1 Theory on micro-mixing model

Turbulent reacting flows are still calculated numerically using Reynolds-Averaged Turbulence models (RANS = Reynolds-Averaged Navier-Stokes). Here the computational grid is not fine enough to resolve the small scale turbulent structures. The length scales for species transport are different for liquids and gases. Therefore models for computational fluid dynamics (CFD) of turbulent reacting gas flows are actually established very well, also in commercial CFD software. To incorporate the influence of the different length scales relevant to mixing and reacting behavior in liquids compared to gas flows a set of additional model equations is needed. These are called micro-mixing models.

The principal difference in mixing of gas flows and liquids becomes clear from turbulence theory. The smallest length scale of turbulent transport of momentum is called the Kolmogorov length scale, η .

$$\eta = \left(\frac{\nu^3}{\epsilon} \right)^{\frac{1}{4}}$$

where ϵ the average rate of energy dissipation per unit mass, and ν is the kinematic viscosity of the fluid. The Batchelor length scale λ_B is the smallest length scale relevant for transport of matter. Below the Batchelor length species transport is only made by molecular diffusion. In turbulence theory it is derived, that the Batchelor scale is proportional to the Kolmogorov scale. The constant of proportionality is the dimensionless Schmidt number. The Schmidt number, Sc is the ratio of diffusive transport of momentum and matter.

$$\lambda_B = Sc^{-1/2} \eta, \quad Sc = \frac{\nu}{D_{mol}}$$

Bachelor Length for Gas and Liquids:

$$\begin{array}{lll} \text{Gas:} & Sc \sim 1 & \rightarrow \lambda_B \sim \eta \\ \text{Liquid:} & Sc \sim 1000 & \rightarrow \lambda_B \sim 0,03 \eta \end{array}$$

So it is easily shown, that the Bachelor length in liquids (with high Schmidt number) is two orders of magnitude smaller compared to gases. This means transport effects of species and mixing on much smaller length scales is influencing the mixing and reaction behavior. This difference is incorporated in the micro-mixing models. Without a micro mixing model numerical simulation of liquid reacting flows with the same models like for gas flows would predict too much reaction yield, because the limiting influence of local mixing time and length scales on the reaction is not included. This means local mixing quality on small length scales is over-predicted.

Turbulence properties like turbulent kinetic energy and turbulent dissipation rate are major influence parameters for the use of micro-mixing models. This means the results will be influenced directly by the accuracy of the turbulent flow calculation. Because these influencing parameters are nonlinear connected to the micro-mixing model, the direct prediction of accuracy or uncertainty is not possible with the investigation of k and ε solely. As a first step a simplified approach can be followed to investigate the influence of turbulence properties on micro-mixing behavior. It is proposed by Prof. Fox e.g. in (R.O. Fox, 2003) and (Liu. Y, 2006).

Micro mixing rate can be defined as suggested by Prof Fox (R.O. Fox, 2003) is

$$\text{Micro mixing rate, } \gamma = \frac{C_\varphi \varepsilon}{2k}$$

In literature it is often assumed, that C_φ is a constant parameter. Prof. Fox has shown a significant dependence of the turbulent Reynolds number and proposes a polynomial function for $C_\varphi(Re_T)$. The derivation is shown in [Liu. Y, 2006] and the proposed function is implemented. Referring to Liu. Y, 2006, the C_φ function of Prof. Fox for the micro-mixing rate can be defined as below

$$Re_T = \frac{k}{\varepsilon \nu},$$

$$C_\varphi = \sum_{n=0}^6 a_n (\log Re_T)^n \quad \text{for } Re_T = 0.2$$

where, a0= 0.4093 a1= 0.6015 a2= 0.5851
 a3= 0.09472 a4= -0.3903 a5= 0.1461
 a6= -0.01604

So it is possible to calculate local values micro-mixing rate inside the complete geometry, if the turbulence properties are known. But micro-mixing is only relevant in regions, where the species are already mixed macroscopically. This means e.g. in the mixing layer of a jet flow (see Figure 2-1).

First investigations have shown large differences in the turbulence properties of the different turbulence models close to the walls. If no mixing is happening close to the wall, these model uncertainties or numerical errors will not affect the prediction of mixing behavior and reaction rate much. So a corrected micro mixing rate is calculated to evaluate better local differences between different turbulence model results and influence on the mixing behavior.

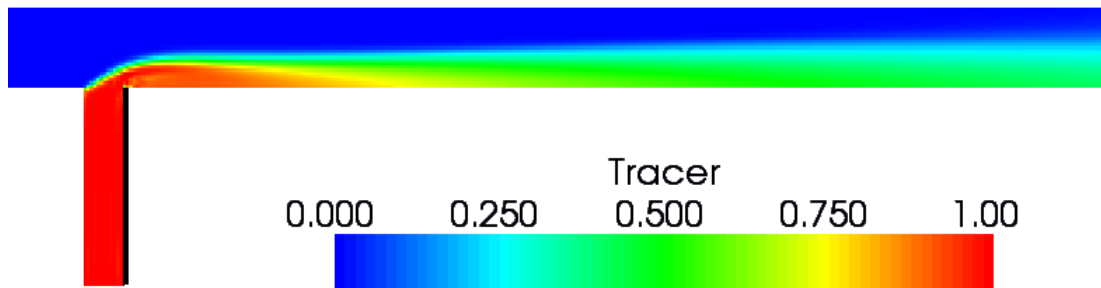


Figure 2-1: Concentration field of a passive scalar inside a T-junction

2.2 Application of turbulent mixing

In recent years, there is an increasing interest for applying process design through the use of the small flow channels to reduce the dimension towards the scale of micro-mixing, leading to process intensification, simplified scaling and hence shorter development times (Hessen et al., 2005). He proposed that the mixing in micro-channels help to promote the mixing process, in which the mixing of the reactants

occurs in ~10 to ~100 μm wide channels. Considering the advantages of the mixer mentioned above, an expected fast liquid mixing may be achieved in the confined channel at millimeter scale. On one hand, the small scales of the streams make it easy to reduce the segregation of the two liquid streams by the turbulent mixing. On the other hand, the mixing process in the millimeter channels can be operated at large flow rates with acceptable pressure drops for mass production of chemicals.

The interaction of turbulent mixing and fast chemical reactions has been investigated in depth by a few research groups. For example, a series of articles by the group of Fox (Y. Liu, 2006 and A. Gokarn, 2006) have made contributions in this area. They applied particle image velocimetry (PIV) and laser induced fluorescence (LIF) technique to reveal the simultaneous velocity and concentration fields in the turbulent mixing process, and several simulation methods based on the micro mixing models. Although great efforts have been made on this topic, there is still a demand for a deeper understanding on the reactive mixing.

Coaxial jet mixers being rather simple engineering facilities find widespread use in different branches of industry and permit realizing the mixing process when conditions for combination of laminar and turbulent flows are regulated through their flowrate ratio. There are a lot of possible mixing regimes. In the paper of Egon Hassel (2005), the author suggested the classical jet mixer (see Figure 2-2) consisting of a nozzle of diameter d positioned along the center line of a pipe of diameter D to study the flow properties. Depending on the flow ratio \dot{V}_D/\dot{V}_d there are two main mixing modes which are r-mode ('r' for recirculation) and j-mode ('j' for jet). The r-mode flow regime has strong recirculation and separation zone close to the nozzle and between the mixing layer and pipe walls. The r-mode condition is $D/d > 1 + \dot{V}_D/\dot{V}_d$ where there appears the mixing regime with a recirculation zone that develops just behind the nozzle near the mixer walls. The r-mode regime involving multiple interactions between initial components and a mixed medium excludes its application in chemical reactors with competitive chemical reactions (K.H. Tebel, 1988). In such reactors, it is important to avoid undesirable competitive reactions since reaction products can interact with initial substances, thus decreasing the yield of desired product. For this not to occur, condition of $D/d < 1 + \dot{V}_D/\dot{V}_d$ must hold true which Barchilon and Curtet (1964) and Henzler (1978) suggested that the flow is similar to

a free jet regime, henceforth, this regime will be called the j-mode. And when the jet and the co-flow mixed, there will be no backflow or recirculation zone.

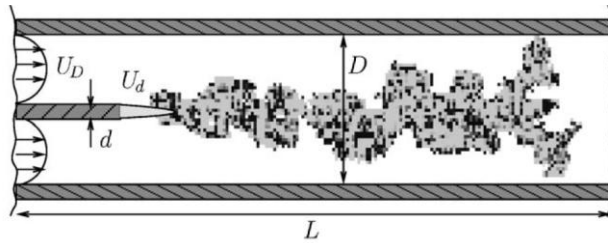


Figure 2-2: Sketch of a jet mixer [Tkatchenko, 2006]

The complex flow field structure in coaxial jet mixers was already investigated by a few researchers like Barchilon and Curtet (1964). A number of works (see Villiermaux and Rehalb, 2000; Mortensen et al., 2003; Lima and Palma, 2002) were devoted to the mixing of an inner slow jet confined by an outer faster one at small Reynolds numbers. These investigations had been motivated by two following problem: (i) the stabilization of the flame front and (ii) the saturation of air co-flow with the molecules of substances transferred by internal jet. Investigations of jet mixers with emphasis on the jet mixer as a chemical reactor are presented in Guiraud et al. (1991), Kruis and Falk (1996) and Baldyga and Bourne (1999) [refer paper Egon Hassel]. Unlike the papers mentioned above we investigate fully developed turbulent flows of the jet mixer both in the r-mode and in the j-mode. Simulation of complex flows in a coaxial jet mixer also had been studied using numerical LES and unsteady RANS models by Igor Tkatchenko et. Al (2006). The studied shown that, the SST model is the most accurate one among the RANS models and the it predicts the mean profile of the mixture fraction for j- and r-mode close to LIF measurements. Also the URANS models fail to predict the unsteady character of the flow.

In order to deeply understand the mixing phenomena in millimetre sized channels, Reynolds averaged Navier-Stokes (RANS) models was chosen to simulate the detailed flow fields and the process of species mixing. Numerical flow simulations of liquid turbulent flows inside mixing nozzles in industrial scale are still mostly done with RANS turbulence models. They do not resolve all scales of turbulent vortex structures but provide useful results with feasible amount of computational power. Engineers are normally interested in knowing just a few quantitative properties of turbulent flows, such as the averages forces on a body or its distribution, the degree

of mixing between incoming streams of fluid, and the amount of a substance that has reacted (J.H. Ferziger, 2002)

The large eddy simulation (LES) approach gives best captured the turbulent flow field and the scalar mixing characteristics, but it is known that the LES method is computationally costly and highly demanding. Using RANS, the computational costs can be reduced by solving the statistically averaged equation system that makes them already a useful tool in industrial design (JurijSODJA, 2007). Refer to J.H. Ferziger, 2002; RANS equation is referring to any averaging processes applied to the Navier-Stokes equations. And in this approaches to turbulence, all of the unsteadiness is averaged out i.e. all unsteadiness is regarded as part of the turbulence. It is possible to derive equations for the higher order correlations, but it still contain more unknown correlations that require modelling approximations, which called turbulence models in engineering.

In this work, the liquid is assumed to be incompressible and miscible. The governing equations are the Navier-Stokes equations, the continuity equation and the transport equation for the mixture fraction. The continuity equation, the Reynolds averaged Navier-Stoked equation and the transport equations for the mixture fraction f are

$$\frac{\partial \bar{u}_i}{\partial x_i} = 0 ,$$

$$\frac{\partial \bar{u}_i}{\partial t} + \frac{\partial \bar{u}_j \bar{u}_i}{\partial x_j} = -\frac{1}{\rho} \frac{\partial \bar{P}}{\partial x_i} + \frac{1}{\rho} \frac{\partial}{\partial x_j} \left[\mu \left(\frac{\partial \bar{u}_i}{\partial x_j} + \frac{\partial \bar{u}_j}{\partial x_i} \right) - \overline{\rho u_i' u_j'} \right] ,$$

$$\frac{\partial \bar{f}}{\partial t} + \frac{\partial \bar{u}_j \bar{f}}{\partial x_j} = \frac{1}{\rho} \frac{\partial}{\partial x_j} \left[\frac{\mu}{Sc} \frac{\partial \bar{f}}{\partial x_j} - \overline{\rho u_j' f'} \right] ,$$

where quantities denoted with $\bar{\quad}$ correspond to time averaged ones, u_i is the i -th component of velocity, P is the pseudo-pressure $P = p - \frac{\rho}{3} \overline{u_k' u_k'}$, ρ is the density, μ is the dynamic viscosity, Sc is the Schmidt number, $\overline{\rho u_i' u_j'}$ and $\overline{\rho u_j' f'}$ are the modeled turbulent stress tensor and turbulent scalar flux vector, respectively.

So far as the overall flow fields were concerned, the predictive mean velocity data obtained by CFD simulations for conventional geometrical configurations showed quantitatively good agreement with experimental data, in use of the standard $k-\varepsilon$ model (Y.N. Chiu, 2009). The ε -equation has severe limitations in the near-wall region. The $k-\varepsilon$ models leads to an over prediction of the turbulent length scale in flows with adverse pressure gradient, resulting in high wall shear stress. The shear stress transport (SST) model proposed by Menter, 1993 allows the disadvantages of the $k-\varepsilon$ model to be overcome. The SST model is based on the gradient diffusion assumption and it combines the best properties of ($k-\varepsilon$) and ($k-\omega$) models. The detail description of the SST model can be found in Igor, 2006. In the simulation from Igor Tkatchenko, 2006 on complex flow in a coaxial jet mixer, it was found out that, a verification based on the comparison with LIF and LDA measurement in the experiment shown that the SST model is the most accurate one among the RANS model. The third RANS model used in present paper is Reynolds stress (RSM) model proposed by Launder et al. RSM is a second-moment closure and it reproduces the anisotropic property of turbulent flow. The detailed information about transport equations and constant of the RSM model can be found in Launder et al., 1975. Hence, three types of models were used in this study which is the standard $k-\varepsilon$ model, the shear stress transport (SST) model, and the Reynolds Stress Model (RSM).

Other work performed to improve the predictions of turbulence quantities included grid refinements, particularly for the region which mixing and reaction take place. Apart from the use of coarse grids which led to severe under-prediction of the turbulence level, results obtained using finer grids were encouraging (Y.N. Chui, 2009).

In this project, a validation and assessment was made based on the simulation and experiment done by Zhe Liu 2009 and Igor Tkatchenko, 2006. In the experiment of Zhe Liu 2009, the liquid-liquid mixing process coupled with chemical reactions in a mini-scale jet mixer was visualized by the reactive laser-induced fluorescence (reactive-LIF) technique for a deep understanding of the interplay between the mixing and the simultaneous reaction. The principle was based on the quenching of the fluorescence signal emitted from the Rhodamine-B dye using the mechanism of

Fenton reaction. The purely physical mixing and the reactive mixing were investigated extensively by comparing the concentration fields under different operating conditions, i.e. the different momentum ratios between the jet and the bulk flows, and the different Reynolds number in the mixing channel of a mini-scale mixer. While in the simulation of Igor, calculations have been performed using three Large Eddy Simulation models and three unsteady RANS models. The time averaged mixture fraction and axial velocity are compared with LIF and LDA measurement for both j- and r-modes of the mixer flow. A special attention is paid to the ability of different models to reproduce unsteady effects. The result obtained from this simulation was being validated with the experimental result presented in the paper of Zhe Liu 2009 and Igor Tkatchenko, 2006, to investigate the performance of the turbulence RANS model and the area of its applicability.

CHAPTER 3: METHODOLOGY

In this work, the studies have been divided into two parts; the first part of the study involves the validation of the CFD simulation of a turbulent liquid flow system in a millimeter-scale channel. The second part of the study involves the modeling of coaxial flow in a coaxial jet mixer. The results for both part of the modeling will be compared with experimental data obtained by Zhe Liu, 2009 and Igor Tkatchenko, 2006.

Simulation process in OpenFOAM software basically needs three steps, which are pre-processing, running and post-processing. The overall structure of OpenFOAM can be shown in Figure 3-1 below.

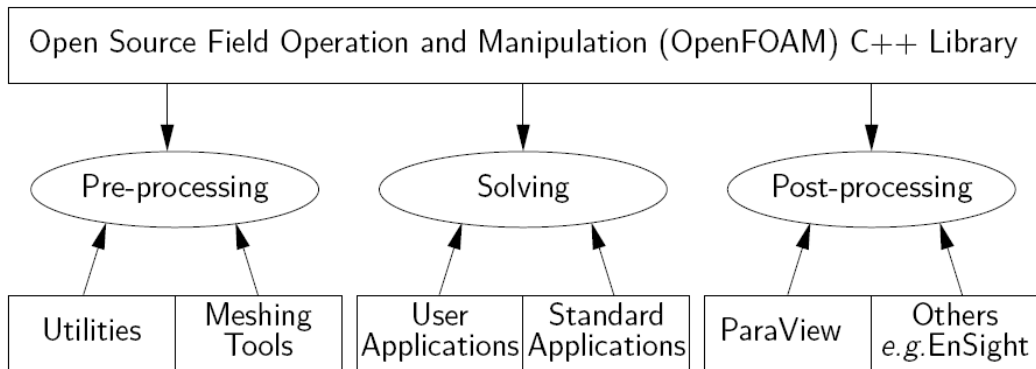


Figure 3-1: Overall structure of OpenFOAM

The core technology of OpenFOAM is a flexible set of efficient C++ modules. These are used to build a wealth of: *solvers*, to simulate specific problems in engineering mechanics; *utilites*, to perform pre- and post-processing tasks ranging from simple data manipulations to visualisation and mesh processing; *libraries*, to create toolboxes that are accessible to the solvers/utilities, such as libraries of physical models.

3.1 Pre-Processing

To start a new case, the first step is to make a geometry dictionary file named *blockMeshDict* and it is located in *constant/polyMesh* directory folder. In this investigation, the file was made using M4 file format because it has the advantage of flexibility in changing the grid size of the geometry. Refer to Appendix A for the details information regarding the M4 format geometry file. Figure 3-2 below shows the geometry of the domains based on the actual geometry size proposed in the literature paper [Zhe Liu, 2009]. The geometry was made in two-dimension in order to reduce the computational cost. Pei-cheng Luo, 2007 concluded that, 2-D simulation can be well accepted to predict the concentration field in the center plane of the mixer geometry. Thus, the following CFD simulations are performed in two-dimension. The channel diameter of inlet A has the same diameter with the mixing zone which is 2mm, while inlet B has diameter of 1mm. And the angle of impingement is 45° between two streams. The conditions of the geometry were chosen referred to the author's previous work on Pi-cheng Luo, 2007. Refer to Appendix A for the detail drawing.

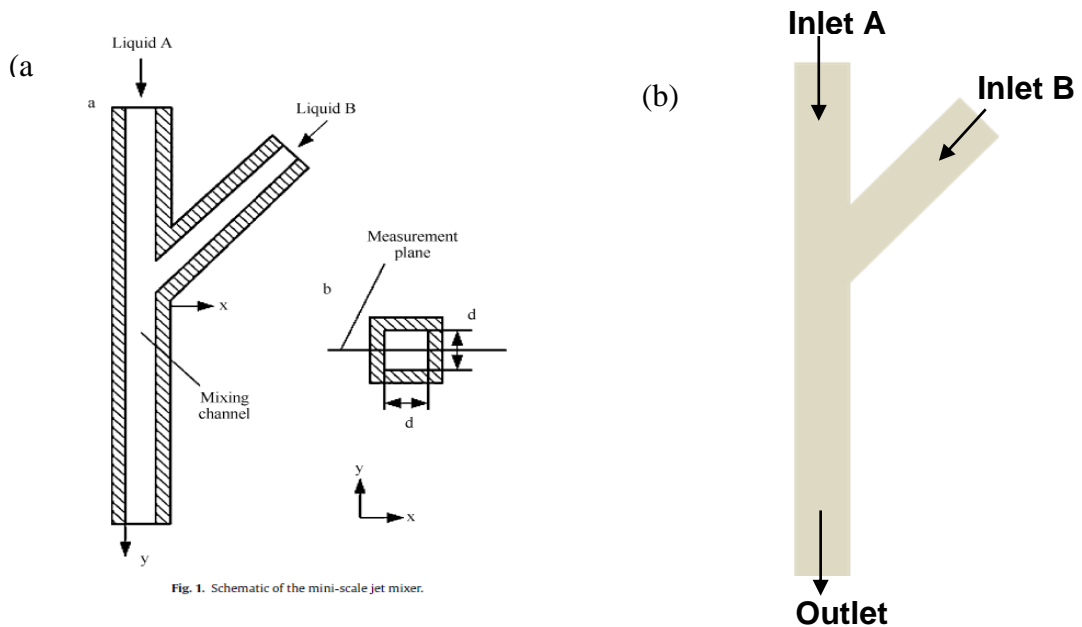


Figure 3-2: (a) Experiment schematic of the mini-scale jet mixer, (b) Simulation domain geometry

In this project, grid sensitivity study also was conducted by assessing the effect of grid size on velocities and turbulent properties. In each case, the grid density was varied from coarse to fine by increasing the number of cells mainly at the mixing zone where a lot important data will be calculated, and also focused near to the wall. The example grid density of the geometry can be illustrated as Figure 3-3. Grid independency was said to be achieved when any further increase in the number of cells did not adversely affect the simulation results; the optimum grid size avoided any unnecessary prolonged computational effort required for the simulations with large number of cells. The grid sensitivity study will be discussed more detail in the chapter 4 of result and discussion.

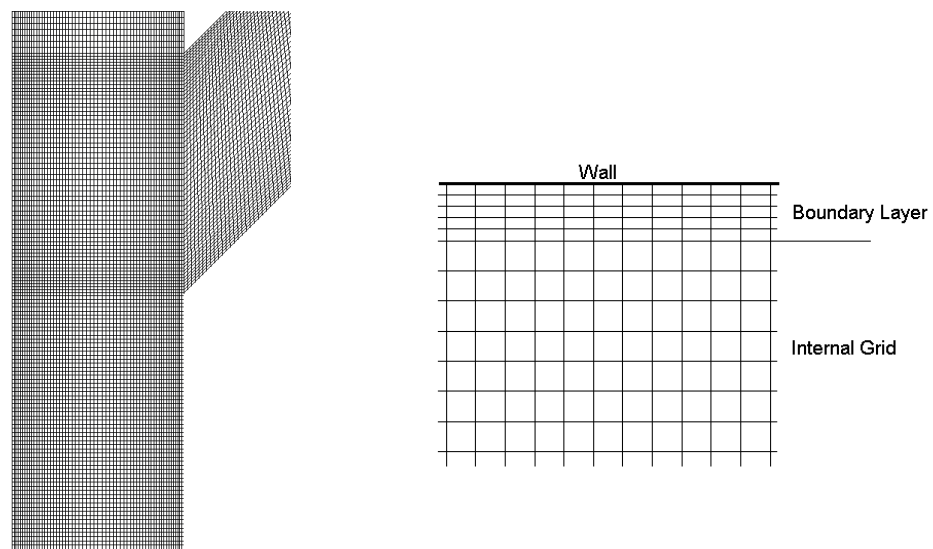


Figure 3-3: Example of grid size (in the picture-coarse mesh)

3.2 Running / Solving

After pre-processing steps, running and solving of the simulation take part. In this step, boundary conditions and operating conditions need to specify to start any simulation. The operating condition was calculated manually referred from the experiment value from the literature. The data used in the experiment can be shown in Table 3-2 which then been calculated to suit in the simulations.

Table 3-1: Operating conditions from experiment

Exp.-II case	Momentum of liquid A [kg ms ⁻²]	Momentum of liquid B [kg ms ⁻²]	Momentum ratio (jet:bulk)	Re number in mixing zone
Phy-4	4.23 x 10 ⁻⁴	4.23 x 10 ⁻⁴	1: 1	1300

The main interest of this simulation was on the study of mixing property in a turbulent flow, therefore the solver used to run this simulation was *simpleFoam* solver which is a steady-state solver for incompressible, turbulent flow of non-Newtonian fluids. To investigate the different behavior of different type of turbulent models, four turbulent models were used which were

- Standard k-ε model
- Realizable k-ε model
- SST k-ω model
- Launder Gibson Reynolds Stress Tensor Model (RSTM)

Standard, realizable k-ε and SST k-ω model are categorized as two-equation models, while the LRR and Launder Gibson RSTM model are categorized as RSTM model. Each model has a different equation applied.

Since it is a steady-state process, ∂t for the simulation is not very important. Therefore, the simulation will be run until it reached a convergence state, where there are no significant changes in the parameters. Therefore, convergence check was done. There are two ways to make sure the simulations meet convergence which is by making residual plot and also check on the monitor points. The monitor point was introduced inside the geometry where changes can be observed and a plot of parameter versus iteration time can be produced. Convergence can be achieved if the monitor point shows constant value after a few number of iteration steps. And the acceptable residual value can be near 1e-6 or 1e-7. The result on the convergence check can be shown in Chapter 4.1.

In order to save the computational time, it is very good if we can strategize the simulation method, so that we can achieve an efficient and fast simulation time. Appendix C describes the strategy used during the simulation in this project.

3.3 Post-Processing

Several utilities were used for post-processing, for example are, *paraview*, *gnuplot* and *octave*. The most frequent utility used was *paraview*. It was used to produce contour plot for all parameter. Here we can observe the characteristic of the flow qualitatively. And to see the results using *paraview*, the data needs to be converted first into .vtk file format. It can be done by typing '*foamToVTK*' in the command line. Refer to Appendix D.2 to see the graphic user interface of *paraview*.

To observe the results quantitatively, we need to make a line plot. The *Gnuplot* version 4.2 utility was used in making the line plot. Each version of *gnuplot* is specific because for different version, it has different types of commands. The details of *gnuplot*'s command line can be shown as in Appendix D.1.

Several locations of sample lines were taken to make comparison between each models, grid sizes and experimental data. So, sample lines were taken using *sample* utility and this data will be used with *gnuplot* to produce the line plot. Besides that, for making mathematical calculation purposes, *Octave* program was used. This program has a similar function with Matlab but Octave is an open-source software. One of the applications with using Octave was the calculation of magnitude velocity of the flow. The mathematics code in Octave can be view as below,

```
1
2 inU=load ("U");
3
4 x=inU(:,1);
5 ux=inU(:,2);
6 uy=inU(:,3);
7 uz=inU(:,4);
8
9 magU=sqrt(ux.^2+uy.^2+uz.^2);
10 data = [x, magU];
11
12 save -ascii magU_coll1.xy data
13
14 clear all;
15
```

On the next part, more details on the result will be discussed.

3.4 Simulation Setup for Coaxial Flow Case

In this case, the simulation was running using the open-source CFD tools called OpenFOAM (Open Field Operation and Manipulation) software. According to Håkan NILSSON 2006, the OpenFOAM results proved to be comparable with results from all the major CFD tools on the market, and it is able to generate good computational results in an efficient way.

The experimental domain of the coaxial jet mixer can be illustrated as in Figure 2-2. Numerical calculations were carried out in a computational domain with the length of eight diameters of the pipe ($L=8D$) and the diameter ratio of $D/d=5$. The diameter of the pipe has 50mm ($D=50\text{mm}$) while the inlet small nozzle has a diameter of 10mm ($d=10\text{mm}$), which gives the total length of the pipe to be 400mm ($L=400\text{mm}$). In order to achieve accurate results relative to the experimental results, 3D structure of domain was used. Figure 3-4 shows the illustration of the domain structure. The computational domain size has $8 \times 2\pi \times 0.5$ in terms of D . In a cylindrical coordinate system (x, θ, r) the grid contains N_x cells in axial, N_θ in circumferential, N_D and N_d in radial directions, i.e., along the diameter of the pipe N_D and the nozzle N_d . In the simulation of Igor Tkatchenko 2006 has tested using the grids of $N_x = 256$, $N_\theta = 64$, $N_D = 32$, and $N_d = 6$. However, in this study, refinement has been made to the grids in order to reach high level of accuracy to the simulation results, and the grids used in this study has $N_x = 280$, $N_\theta = 80$, $N_D = 70$, and $N_d = 30$. The edge-grading and the grid structure strategy was used as shown in Figure 3-4 (b) to minimize the cell skewness and aspect ratio, also to create a uniform meshes especially in the center of the nozzle and pipe where there is many information calculated during the simulation. Refer to Appendix B for the detail drawing of the coaxial jet mixer.

The simulation was assumed to be incompressible flow which means the density of the fluid will be constant and the fluid used in the simulation was assumed to be water. It was also noticed in Valery Zhdanov 2004, that the mixing was not influenced by the temperature factor $(T_D - T_d)/T_D$. Both j-mode and r-mode regimes were simulated at the Reynolds number of $Re_d = 10^4$. The flow conditions adopted in the simulations are listed in Table 3-2, where the velocity inlet of the nozzle and pipe were calculated based on the flow rate ratio, Q and the Reynolds number Re_d .

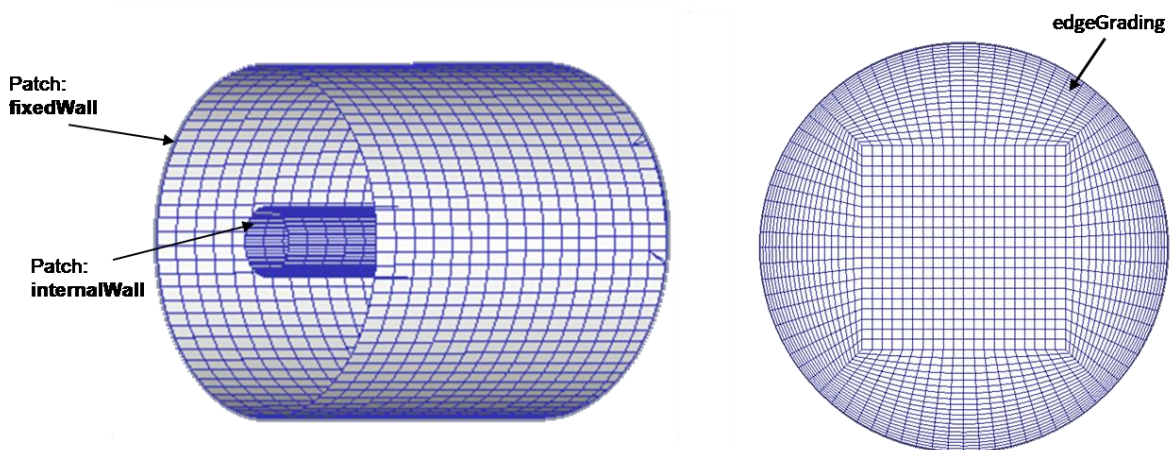


Figure 3-4: The 3D domain structure (left) and the mesh grading of the inlet nozzle (right)

Table 3-2: The flow conditions adopted in the simulation

	R-mode	J-mode
Flow rate ratio, $Q = \dot{V}_D/\dot{V}_d$	1.3	5
Volume flow rate (m^3/s)	$\dot{V}_D = 1.021e^{-04}$ $\dot{V}_d = 7.854e^{-04}$	$\dot{V}_D = 3.927e^{-04}$ $\dot{V}_d = 7.854e^{-04}$
Velocity (m^2/s)	$u_D = 0.054$ $u_d = 1.000$	$u_D = 0.208$ $u_d = 1.000$

CHAPTER 4: RESULTS AND DISCUSSION

In the simulation of solving a physical fluid flow, the technique used was by breaking down the physical domain into a large number of discrete control volumes, called elements or cells. Discretization of these elements or cells is probably the most crucial source of error for the accuracy of numerical fluid flow simulations (Michael Casey, 2000). Therefore, two parameters have been study to control the numerical error which is convergence check study and grid sensitivity.

4.1 Convergence Check

During the solution procedure, it is often preferred to have the residuals for the various equations plotted as function of iteration number. By doing so it is possible to visualize how the residuals are developing with iterations. As been suggested in Micheal Casey, 2000; in the simulation process, the parameters used to control the level of convergence are by varying relaxation factors, damping factors or time steps. In this study, time step or iteration step was been used to control the convergence factor. Other than that, by using monitor points, a specific location of interest will be examine on the time-development of the physical quantities which can identify whether the flow is steady or not.

The values of the variables were evaluated at different number of iterations in the point (0.001, 0.02, 0.0). This point is depicted in Figure 4-1. The location was taken because it is located in the mixing zone which seems like a good point to check whether the solution converged.

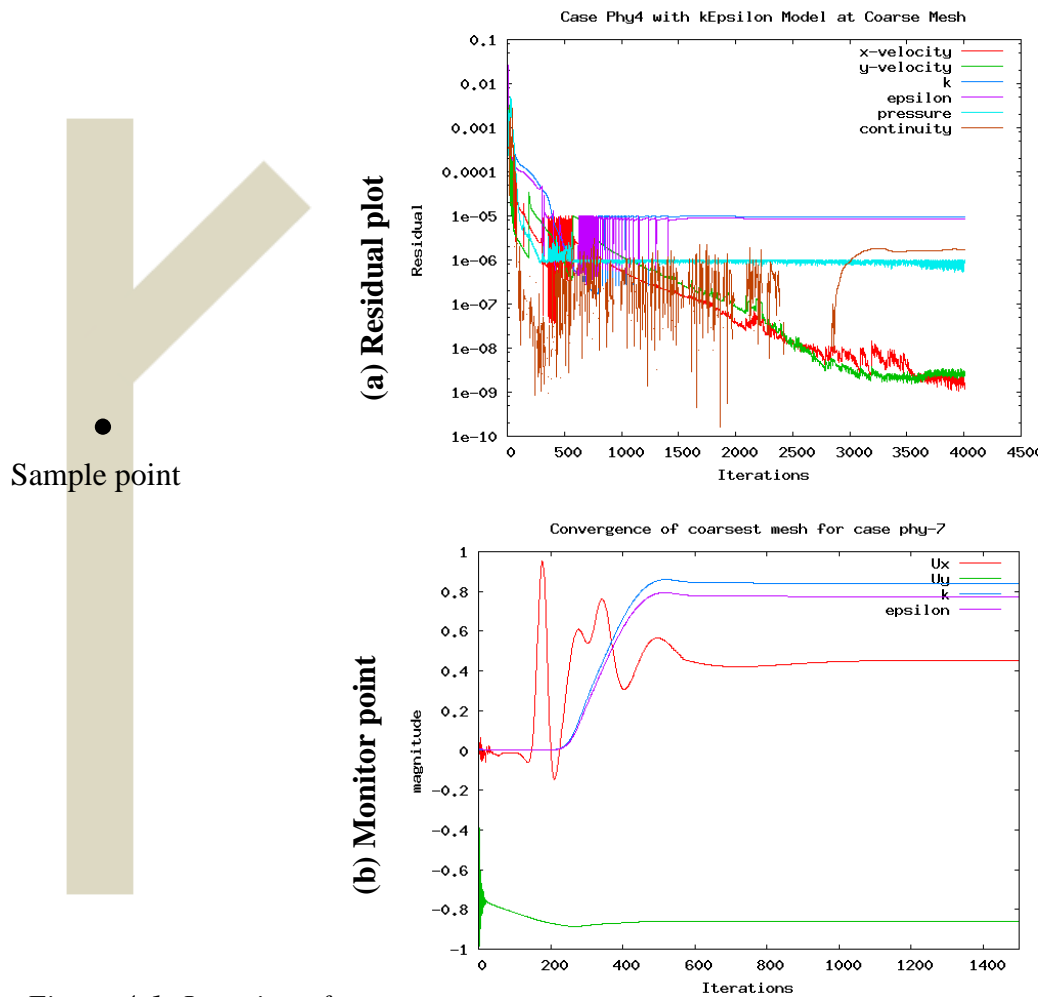


Figure 4-1: Location of sample point for observation of the convergence

What is seen on the residual curves is that the residuals are reduced to a certain level, where after the curves, exhibits random fluctuations. These fluctuations are caused by the numerical round off errors associated with the CFD codes level of precision.

The other simulations behave in a similar manner. The evaluation of the variables at the sample point helps to make sure that the solution is fully converged. This is important because comparison between simulations would not make sense without convergence of the single cases. It was therefore made sure that the experiments that were carried out will not stop before the solution is sufficiently converged.

Figure 4-1(a) depicts the residuals of the solution of one of the simulations. And Figure 4-1(b) depicts the convergence at the sample point. The values of the variables in this plot were divided by their maximum absolute value to make them fit in one figure. The plots show that the simulation behaves well.

4.2 Grid sensitivity study

Grid sensitivity tests were conducted by assessing the effects of grid sizes on the mean velocities, and turbulent kinetics energy, k . The grid size was varied by increasing the number of cells in x and y direction only (since this is a 2D cases). Grid independency was said to be achieved when any further increase in the number of cells did not affect the simulation results. To make sure the comparison is reliable, two locations were evaluated along the geometry; at $x=1\text{mm}$ and $y=20\text{mm}$ with two different parameters. The locations can be illustrated as Figure 4-2 below.

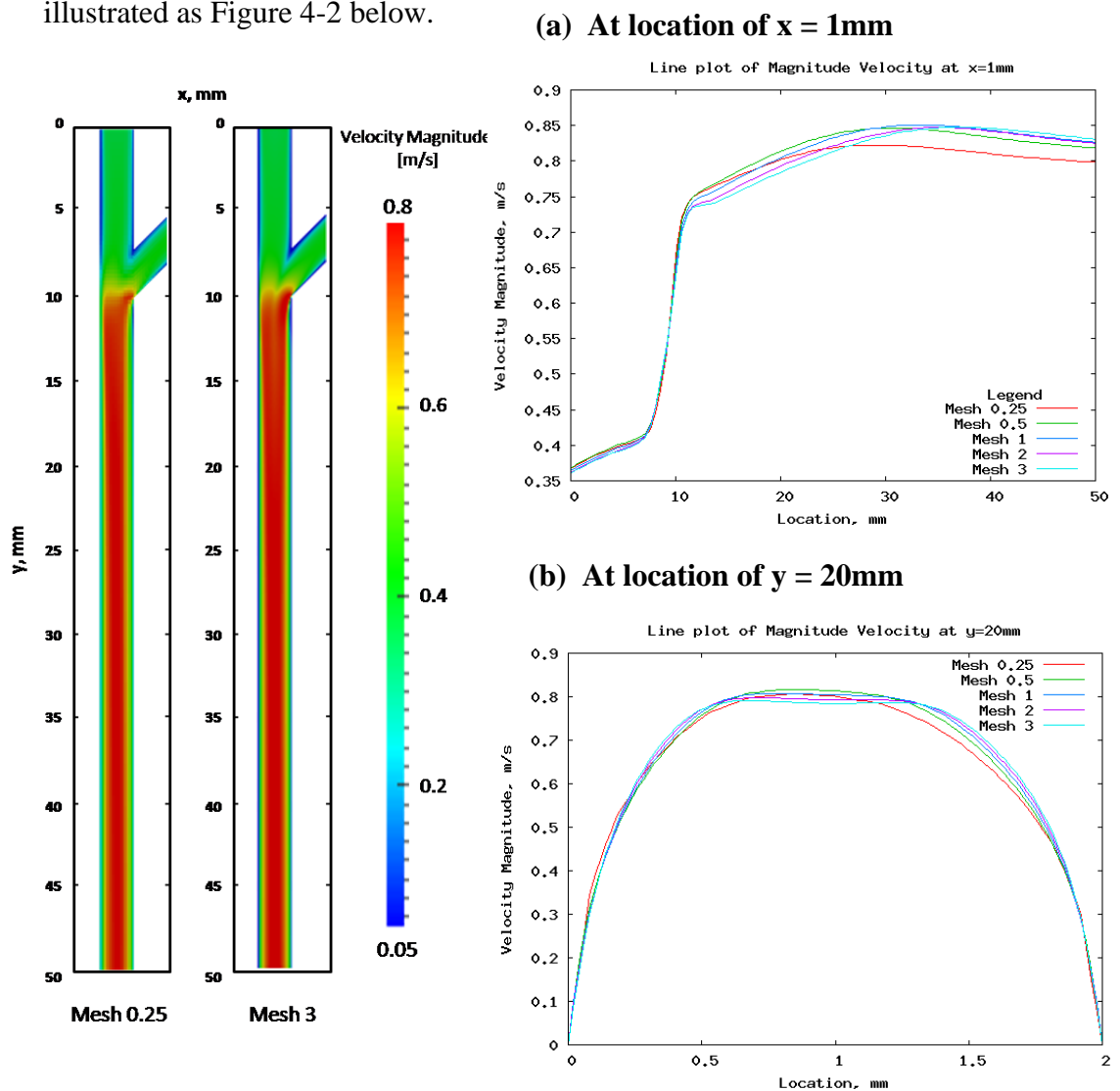


Figure 4-2: Location of line plot with velocity magnitude parameter (a) along x -plane and (b) along y -plane

Results for the line plot for the magnitude velocity can be shown in Figure 4-2, where five types of meshes at two different locations were been plotted. The different size of meshes can be described in Table 4-1.

Table 4-1: List of meshes

Name of mesh	No. of cells	Cells in channel A radius	Grid size in mixing zone [μm]
Mesh 0.25	3, 600	7	142.86
Mesh 0.5	14, 400	15	66.66
Mesh 1	57, 600	30	33.33
Mesh 2	230, 400	60	16.67
Mesh 3	921, 600	120	8.33

Figure 4-2(a) show velocity magnitude (m/s) profile along the x-direction in the center of the channel, and Figure 4-2(b) shows also the velocity profile along the y-direction which both have been plotted against distance from inlet channel until the outlet. In these two plots, mesh 0.25 which is the coarsest mesh behave very differently from the other meshes, especially the peak near the wall at the location of 40-50 mm. The max spread between the coarsest mesh with the finest mesh is approximately 0.05 m/s.

However, looking only at velocity profiles is insufficient to choose the optimum size of grid because they behave almost similar from each other. It is repeatedly found in many CFD papers that the authors check only on one parameter especially velocity component. Therefore, the parameter of turbulent properties such as turbulent kinetics energy needs to take account. Especially in developing micro-mixing model, the value of k and ϵ are very important, since their value are related to the micro-mixing rate which can effects the results greatly in the calculation of turbulent reacting flow.

Figure 4-3 show two plots of turbulent kinetics energy along (a) x-direction and (b) y-direction; against the location along the channel. From this graph, it tells us that the turbulent kinetics energy does not behave the same way as the velocity magnitude. As the refinement continues, the turbulent kinetics energy deviates differently between the coarsest mesh (mesh 0.25) to the finest mesh (mesh 3). For example is at the location more to the downstream of the channel (outlet) at

Figure 4-3(a). The peak kinetics energy is at the outlet (at $y=50\text{mm}$) which spreads about $0.0025\text{-}0.0048\text{ m}^2/\text{s}^2$ and it is also very sensitive at this region. Also we can observe a great spread at the location of 10mm where the impingement of the two liquids are expected to occur, which gives max spread of approximately $0.0006\text{m}^2/\text{s}^2$ of turbulent kinetic energy, k .

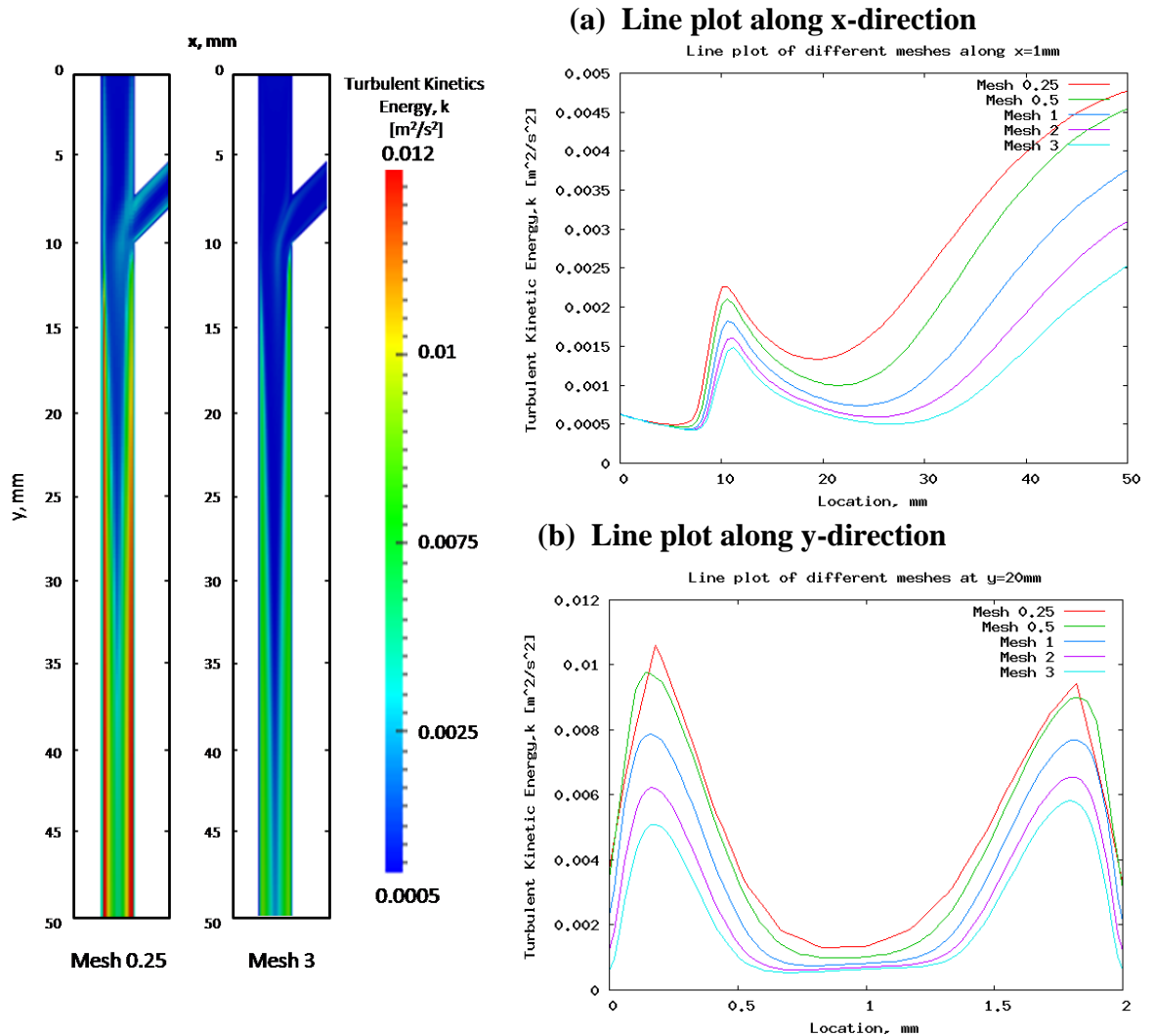


Figure 4-3: Line plot of different meshes at parameter turbulent kinetics energy, k (a) along x -direction; (b) along y -direction

Referring to the plot of k at Figure 4-3(b) along the y -direction, the value of k is low near the wall and also at the center of the channel, specifically at $0.1\text{-}0.2\text{ mm}$ away from the wall with the value around $0.002\text{-}0.004\text{ m}^2/\text{s}^2$. The low value k near the wall happen maybe because of the no-slip boundary condition defined on the wall, which is assumed to have zero k value.

With having low grid density cells (coarse mesh), the computer is said to be over-predicted the value of k , where we can see at Figure 4-3(b) near the wall, mesh 0.25 (which is the coarsest mesh) have peak value of $0.011\text{m}^2/\text{s}^2$. This value gives 120% higher than the finest mesh which belongs to mesh 3. As the refinement increases, the value of k in the center behave almost similar and only have small different, that is less than 2% of the max spread created at the k value near the wall. Mesh 2 and mesh 3 almost behave similar with very insignificant difference. Therefore, mesh 2 is said to be reached grid independent where making finer mesh will not give any significance improvement to the final results. We can also define mesh 2 and mesh 3 as they reached the asymptotic level.

It is also satisfy with the experimental result as shown in Figure 4-5(b) and Figure 4-6. In conclusion, the mesh 2 is already fine enough to reach grid independence and it is reliable to predict the right flow behavior by using mesh 2 grid sizes. With that, the rest of the simulation in this study will only refer to grid size of mesh 2.

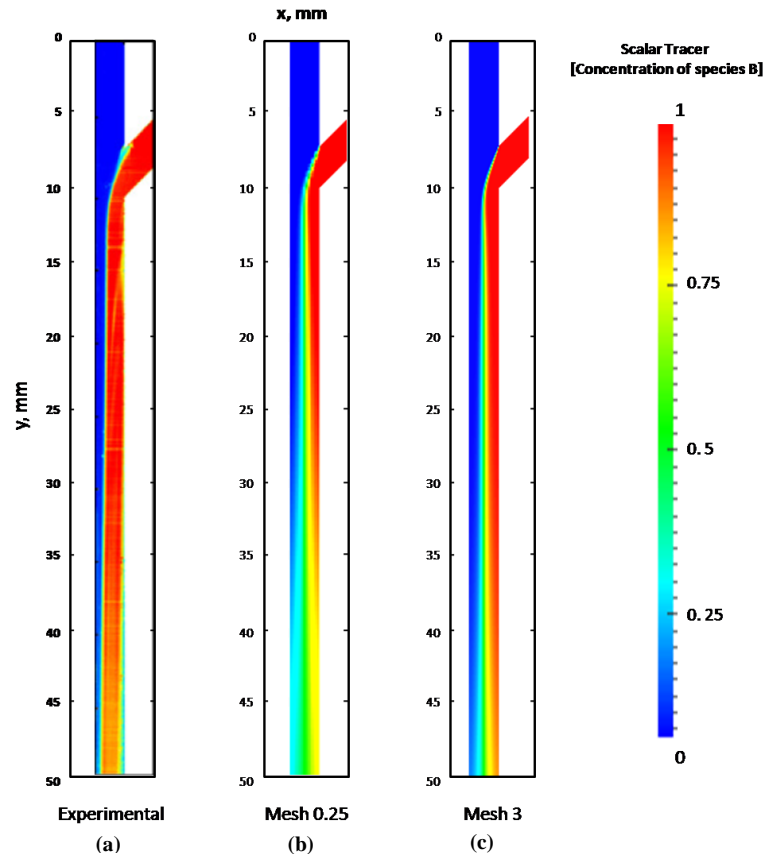


Figure 4-4: Comparison of contour plot between (a) experimental [Zhe Liu, 2009] with the simulation result at (b) mesh 0.25 and (c) mesh 3

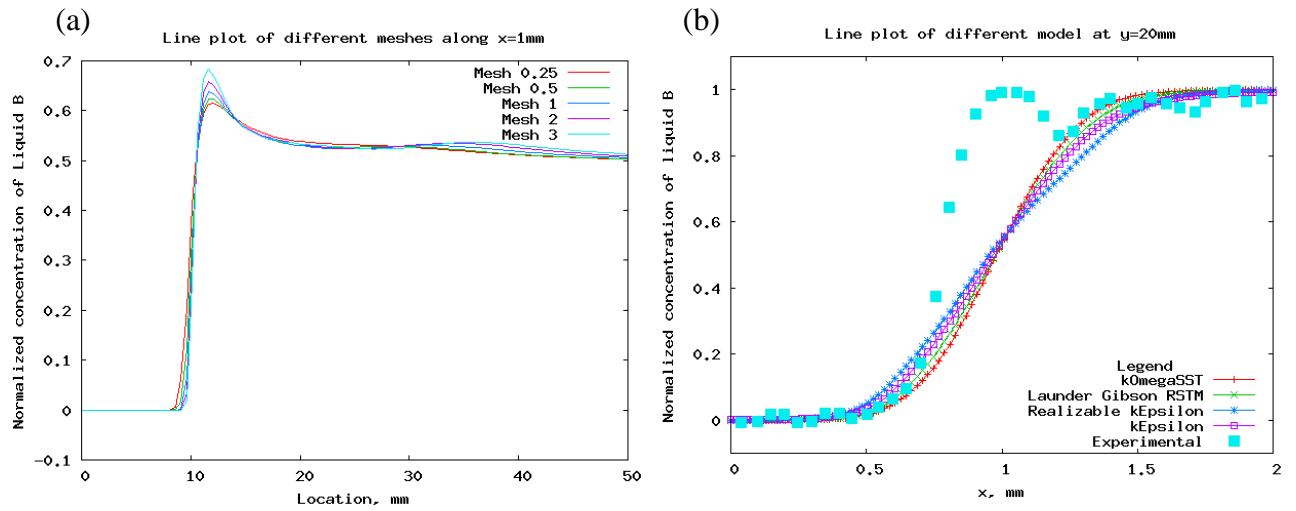


Figure 4-5: Line plot of different meshes at the tracer concentration of species B (a) along x-direction; (b) along y-direction

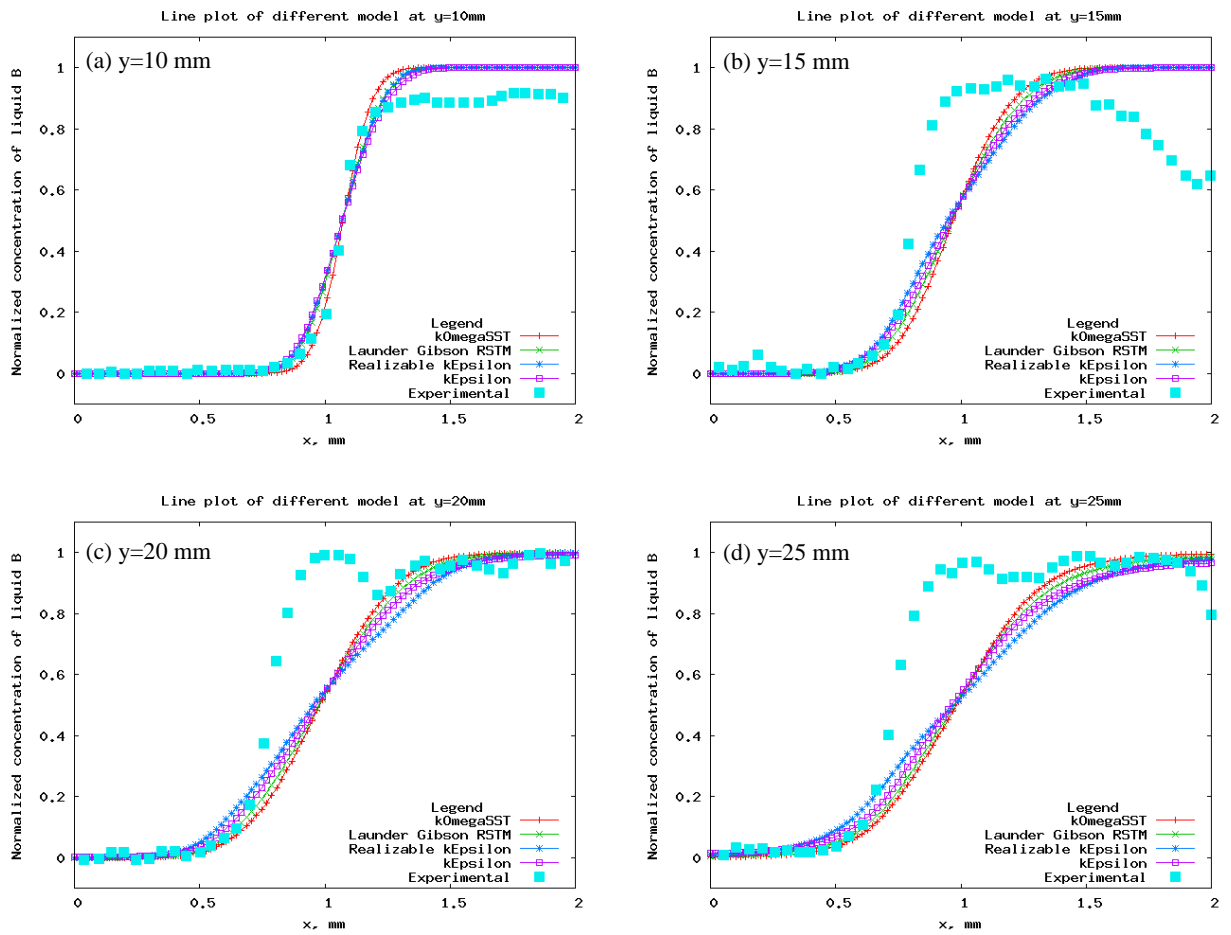


Figure 4-6: Line plot of different meshes at the tracer concentration of species B compared with the experimental data.

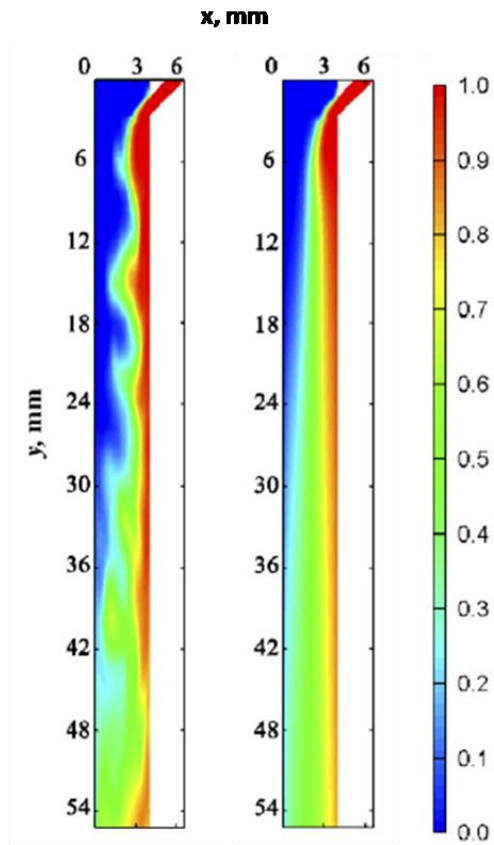


Figure 4-7: Trend result of Y-shape nozzle from Peicheng Luo 2007

Refer to Figure 4-6 we can see that the behavior of flow in the experiment and simulation starts to contradict. These phenomena can be explained by looking on the experimental result near the outlet of the stream, at the right side of the wall (see Figure 4-4(a)). The concentration of mixture suddenly dropped distinctively. That is why we can see low fraction mixture in the plot of Figure 4-6(b) at the location of $x > 1.5\text{mm}$ until the wall. The sudden drop of the mixture fraction shouldn't be happen because it is quite impossible for the stream A to pass through the stream B without diffused. In the experiment done by Peicheng Luo 2007 (see Figure 4-7) , the author used the same nozzle geometry (Y-shape nozzle) but at different flow parameter, the trend of result show no similar with the experimental result by Zhe Liu 2009 (see Figure 4-4) especially at the wall near the nozzle outlet. So, we can say that the experimental result quoted from Zhe Liu 2009 has some inaccurate results and error, and it is also one the reason why the simulation results show distinctive different with the experimental results.

The other possible reason is due to the time where the result is taken. Since the result is a time-averaged result (steady state condition), the data should be taken after the flow reach the steady state condition. Therefore, the other reason of the error maybe because the author take the result at instantaneous time without waiting it to become stable or steady.

4.3 Coaxial Flow Jet Mixer

Table 4-2 show the images of the r-mode and j-mode regimes corresponding to the flow conditions listed in Table 3-2. Colors in these images represent the magnitude velocity and the normalized concentration to observe the mixture fraction that affects from the mixing process in the coaxial jet. The magnitude velocity of the j-mode is higher than the r-mode is due to the higher flow rate ratio of the j-mode scheme. It is also due to the vortices created in the r-mode, near the wall just after the nozzle inlet. These vortices will create a recirculation zone where actually helps for the mixing process. It can be seen at the mixture fraction of the r-mode where the flow is instantly mixed at the location of $x/D = 1.4$. There is no recirculation zone for j-mode to avoid from back mixing to occurred. This type of regime is suitable for the reactive mixing where back mixing can promote side reaction to form which can produce undesired product that is unwanted for a process.

Table 4-2: Simulation results for r-mode and j-mode with respect to magnitude velocity and mixture fraction.

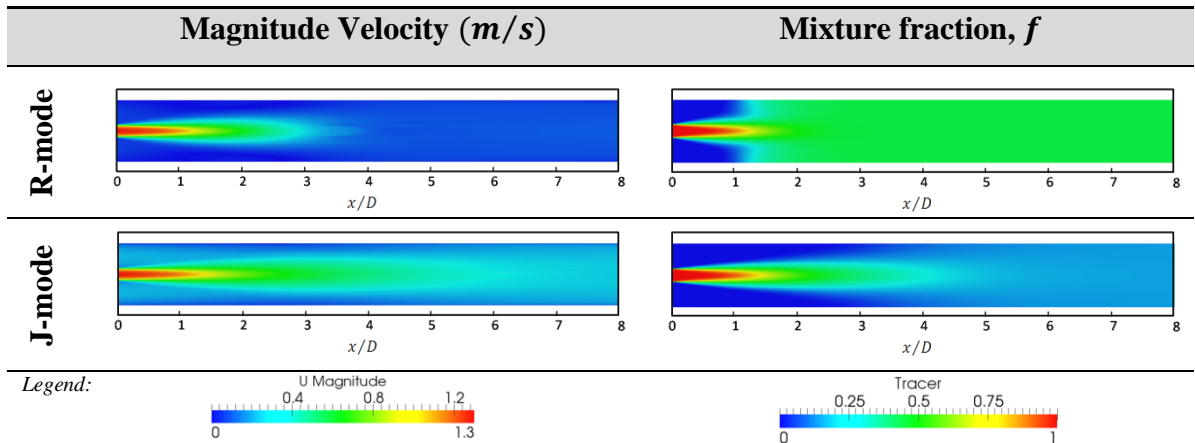


Figure 4-9 plots give more quantitative concentration information along the mixer axis as depicted in Figure 4-8. The simulation results with different models were compared with the experimental data extracted from Igor Tkatchenko, 2006. Through this observation, there are not many different between one to another model. By comparing with the experimental data, both r-mode and j-mode are able to predict the flow correctly only in the middle of the nozzle which located at $x/D < 2$. However, between these two modes, the j-mode can produced data most nearer to the experimental data than we can observe at the r-mode. This is

because the RANS models fail to predict the unsteady behavior of the flow, especially in the r-mode where recirculation is expected to happen.



Figure 4-8: Sample line location along the mixer axis

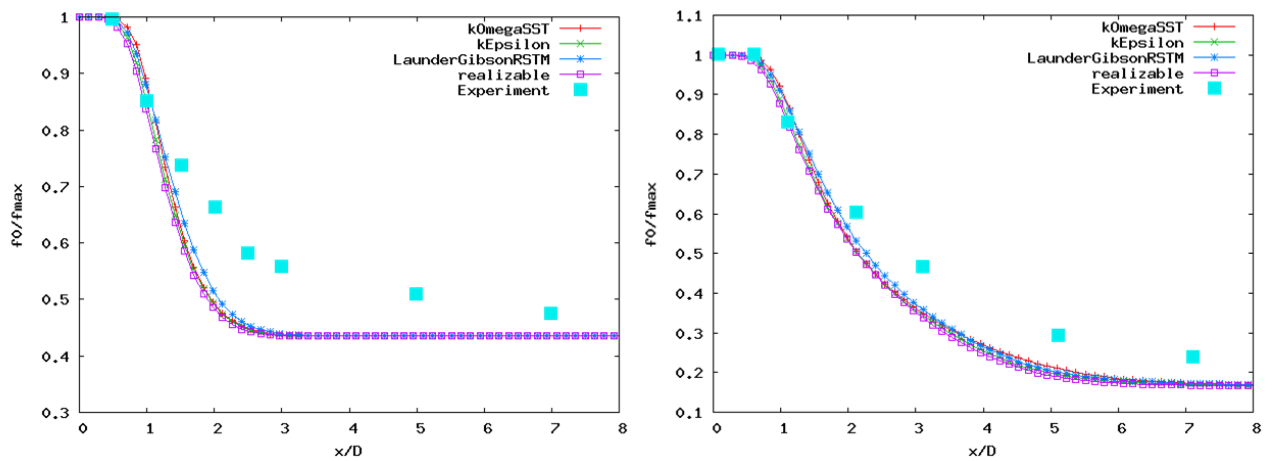


Figure 4-9: The distribution of the mean value of the mixture fraction along the mixer axis R-mode (right) and J-mode (left). f_{max} is the maximal mean mixture fraction in the first cross section $x/D = 0$ and f_0 is the maximal mean mixture fraction on the mixture centreline in the cross section x/D .

Figure 4-11 shows the mean profile of the mixer fraction on the mixer centerline in the cross section of x/D . The radial position also had been plotted as illustrated in Figure 4-10. In the location of $x/D = 1.6$ (see Figure 4-11e), the predicted RANS model at j-mode shows a very good agreement with the experimental data. Some discrepancies between the simulation and experimental are observed for the mixture fraction near the pipe wall for the r-mode (see Figure 4-11a, b, c). A possible reason for underestimation of the mixture fraction at $r/D > 1.5$ might due to the large artificial diffusivity caused by coarse grid resolution. However, it should be noted that the transport of the scalar across the pipe is caused by the radial velocities as proposed by Igor Tkatchenko, 2006. Therefore, another reason for the discrepancy could be a poor prediction of radial velocities.

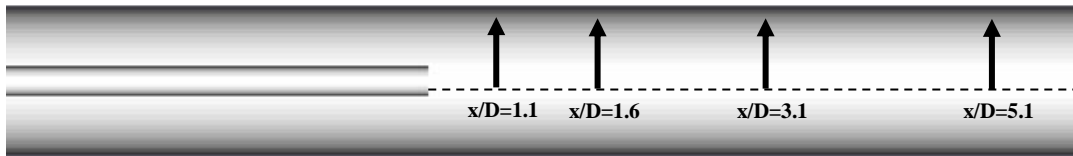


Figure 4-10: Sample line location along radial mixer axis.

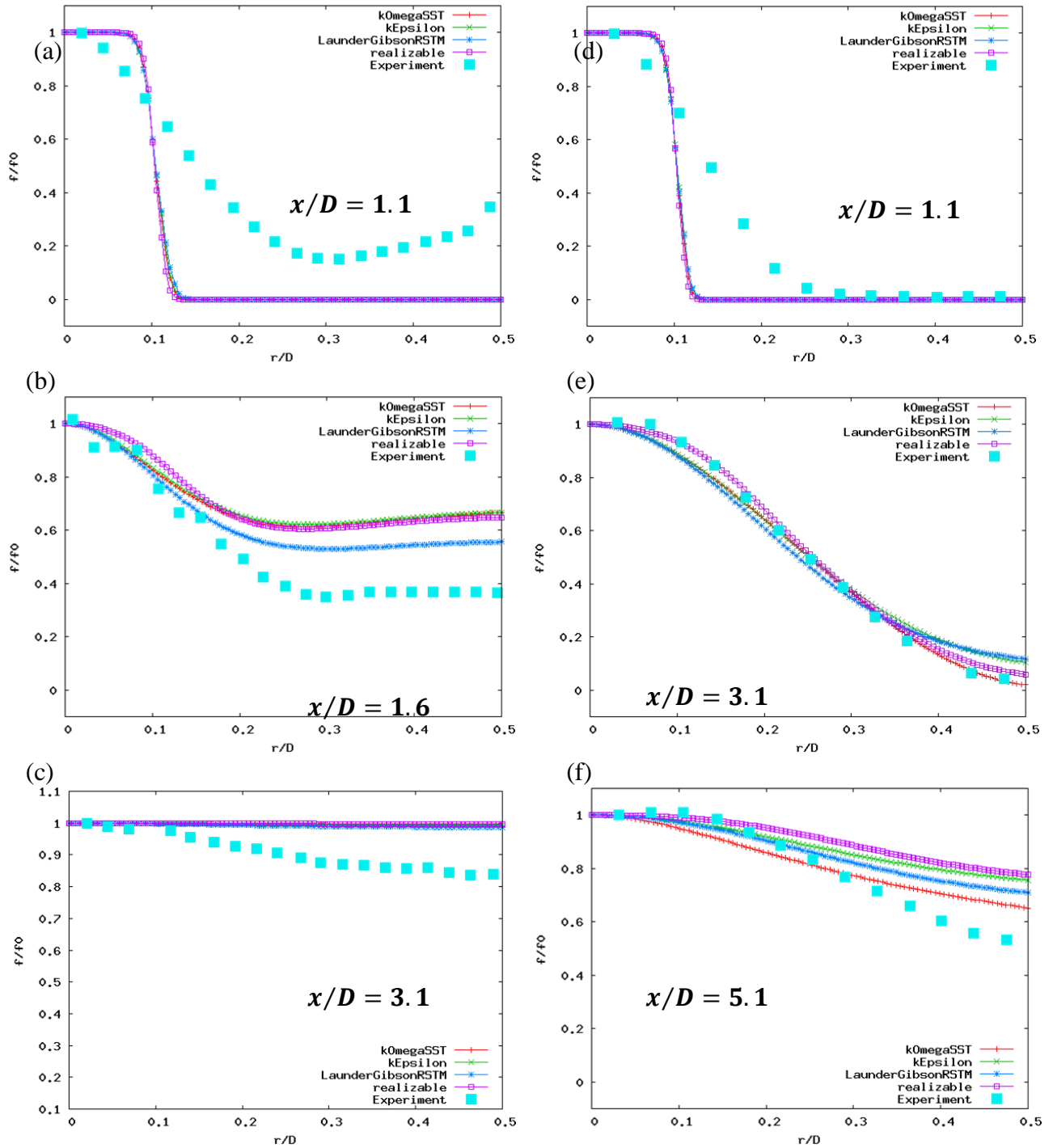


Figure 4-11: The mean profile of the mixture fraction. R-mode: Section (a), (b) and (c). J-mode: Section (d), (e) and (f). f_0 is the maximal mean mixture fraction on the mixture centreline in the cross section x/D .

The next steps of models validation is the velocity analysis. The comparison of the mean profiles at the axial component of the velocity with the experimental measurement is presented in Figure 4-12. Figure 4-12(a), (b), (c) represented the plot at the r-mode regime, while Figure 4-12(d), (e), (f) represented the plot for the j-mode regime with respect to specific x/D locations. Again, the RANS model fails to predict the velocity behaviour at $x/D = 1.1$ in r-mode regime as shown in Figure 4-12(a). However, in j-mode regime, at the location of $r/D > 0.2$, the simulation shows very well predicted with the experimental value.

In order to compare the capability of the turbulent models to predict the right flow behavior, both mixture fraction and velocity plot were observed. Figure 4-11 that show the mixture fraction plot doesn't give sufficient prove to decide which turbulent model has best fit the simulation because almost all the turbulent models give similar results. However in Figure 4-12 that shows the axial component of velocity gives some differences between each turbulent model. The Launder Gibson RSTM model shows a good agreement with the experimental data at location of $x/D = 1.6$ with the r-mode (see Figure 4-12**b, c**) because among the other RANS model, RSTM model has the least assumption in its numerical equation. The standard $k - \epsilon$ model in the other hand is incapable to predict the flow behaviour since its result gives in high discrepancies with the experimental value at the j-mode regime, $x/D = 5.1$ (see Figure 4-12**f**).

In this study also has proven the result of Igor Tkatchenko, 2006 stated that, when the Reynolds averaging is used and the time of averaging ($T_0 = tU_D/L$) increases, the flow patterns tends to the axial symmetric form at least in the central core of the pipe flow. In the Figure 4-9 that show the plot of mixture fraction in the axial direction, it agrees with the experimental data at the early of the flow, near the nozzle ($x/D < 1.8$). However, the flow behaves differently when we observe on the radial direction of the flow. As we can in Figure 4-11 and Figure 4-12, the flow profiles only agree with the experimental data at the location far from the nozzle inlet ($x/D > 1.6$), but not at the early flow near the nozzle which is located at $x/D = 1.1$ (see Figure 4-11(a),(d) & Figure 4-12(a),(d)).

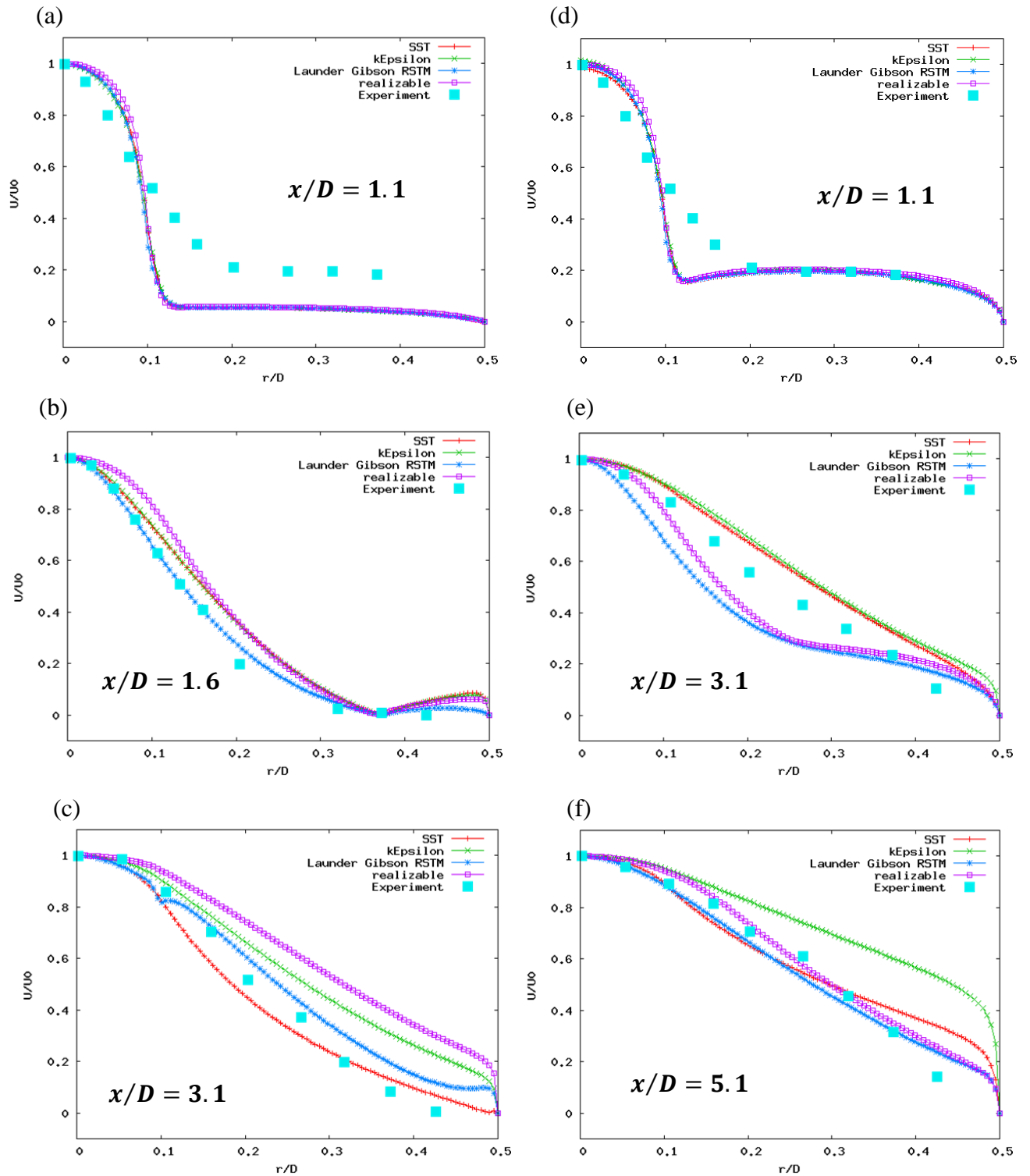


Figure 4-12: The mean profile of the axial component of velocity. R-mode: Section (a), (b) and (c). J-mode: Section (d), (e) and (f). u_0 is the maximal axial velocity on the mixture centreline in the cross section x/D .

CHAPTER 5: CONCLUSION

Flow phenomena in a fast liquid mixing process by the cross-flow impingement of the two thin liquid sheets in the confined mixing channel at millimeters; and a complex flow in a coaxial jet mixer are studied by the CFD simulations with different size of grid and turbulent model.

For the case study of cross-flow impingement of two thin liquid sheets, it can be concluded for the grid study, the velocity profiles in the mixing nozzle are less grids dependent compare to the turbulent properties because as observed from the results, the velocity profile shows almost similar at every grid size. However, for the turbulent kinetics, it does not behave the same way as the velocity magnitude. Therefore, it can be concluded that mesh 2 and mesh 3 have reach their asymptotic level and mesh 2 is chosen as grid independent and believe that it can predict the right flow behavior of fluid in the millimeter channel.

While, for the case of coaxial jet mixer, two flow modes were studied. In the r-mode regime, it is observed that it reached full mixed earlier than in the j-mode which is caused by the help of recirculation zone in the r-mode regime. By looking on the mixture fraction plot, the different between each turbulent cannot really seen because each behave almost similarly to each other. However, it can be seen that the RANS models can predict the behavior of j-mode better than for the r-mode. This is because the RANS model unable to reproduce the vortices of the flow in the r-mode regime especially near the wall. But RANS models give quite good results with the flow where there are no or few vortices like in the j-mode regime.

Velocity profiles of both r- and j-mode also were studied in this case. The results show that the RANS model fail to predict the right flow behavior at the early flow (at $x/D = 1.1$) compared to the experimental data but it gives good agreement at the later of the flow ($x/D > 1.6$). The possible reason is because of the behavior of axial asymmetry of the flow as suggested by Igor Tkatchenko, 2006, stated that the flow patterns will tends to the axial symmetric form in the

central core of the pipe flow. Launder Gibson RSTM model shows the best turbulent model in predicting the flow with vortices like in the r-mode, while SST $k - \epsilon$ model rather good model in predicting the flow in j-mode where there is less or no vortices near the wall.

RANS model is incapable to reproduce the vortices structure in the pipe and nozzle but it capable in predicting the area of mixing and the velocity profile correctly in certain locations. This study can help the engineer in the industry to understand the effects of the flow so that they can predict and focus on the area of the applicability that the RANS model can perform. Knowing the superiority of each turbulent model can help the engineers and researchers in deciding the selection of turbulent model need to be use in order to save the simulation time and also to reduce the errors produced in their simulations.

REFERENCES

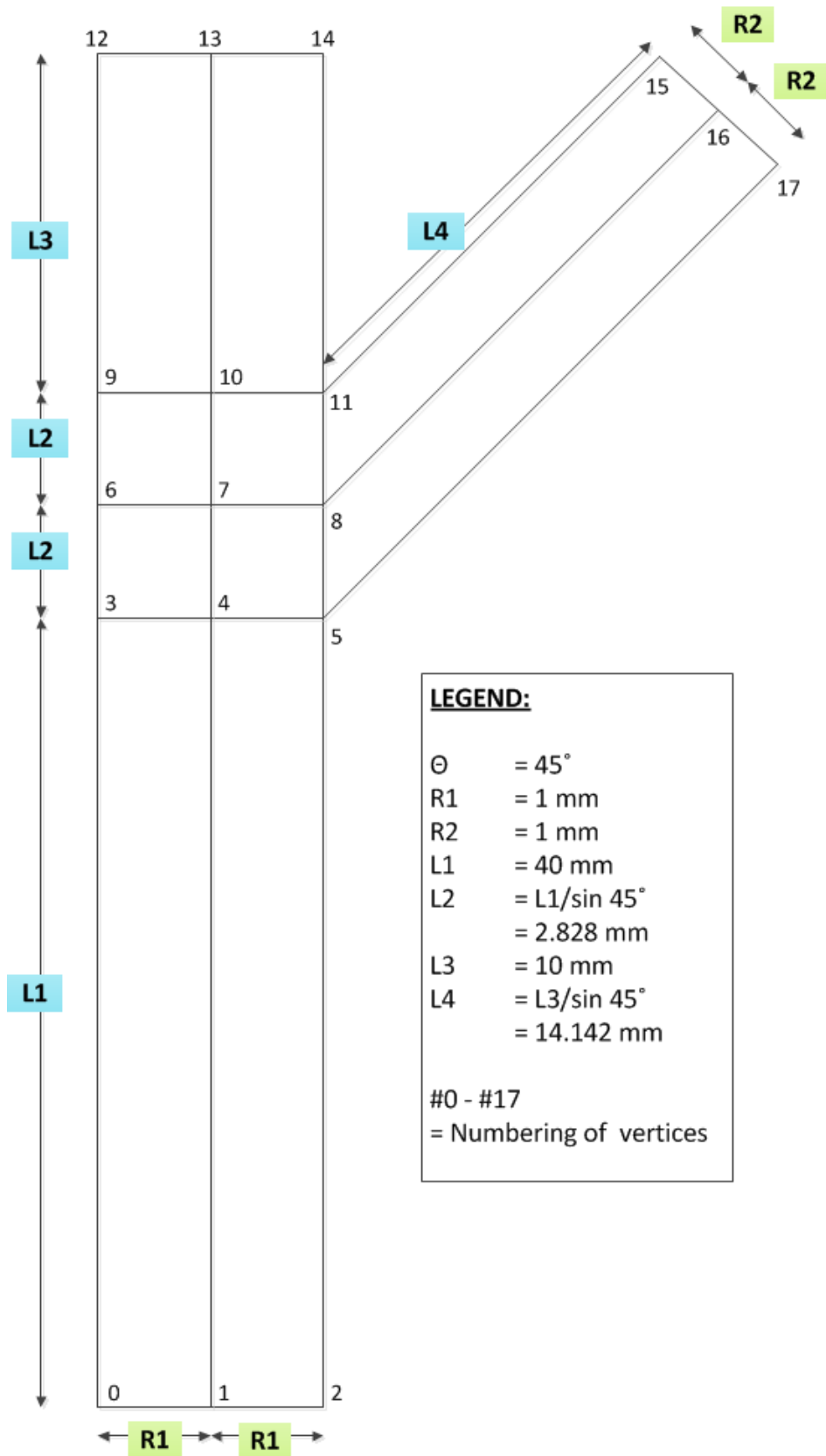
- A. Gokarn, F. Battaglia, R.O. Fox, J.C Hill, *Simulation of mixing for a confined co-flowing planar jet*, Computational Fluids 35 (2006) 1228-1238
- Baldyga, J., Bourne, J.R, 1999, *Turbulent Mixing and Chemical Reactions*, Wiley, New York.
- Barchilon, M., Curtet, R., 1964. *Some details of the structure of an asymmetric confined jet with backflow*. Journal of Basic Engineering 777-787
- B.G. Lakatos, *Population balance model for mixing in continuous flow system*, Chemical Engineering Science 63 (2008) 404-423
- Bourne, J.R., 2003. *Mixing and the selectivity of chemical reactions*. Organic and Process Research & Development 7, 471.
- Brucota, A., Ciofalo, M., Grisafi, F., Toco, R., 2000 on the *Simulation of stirred tank reactors via computational fluid dynamics*, Chemical Engineering Science 55, 291-302
- Egon Hassel, S. Jahnke, N. Kornev, I. Tkatchenko, V. Zhdanov, *Large-eddy simulation and laser diagnostic measurement of mixing in a coaxial jet mixer*, Chemical Engineering Science 61, 2908-2912 (2006)
- F. Schwertfirm, J. Gradl, H.C. Schwarzer, W. Peukert, M. Manhart, *The low Reynolds number turbulent flow and mixing in a confined impinging jet reactor*, Int. J. Heat Fluid Flow 28 (2007) 1429-1442
- Guiraud, P.J., Bertrand, J., Costes J., 1991. *Laser measurements of local velocity and concentration in a turbulent jet-stirred tubular reactor*. Chemical Engineering Science 46, 1289-1297.
- Håkan NILSSON, 2006. *Evaluation of OpenFOAM for CFD of turbulent flow in water turbines*. 23rd IAHR Symposium – Yokohama, October 2006.

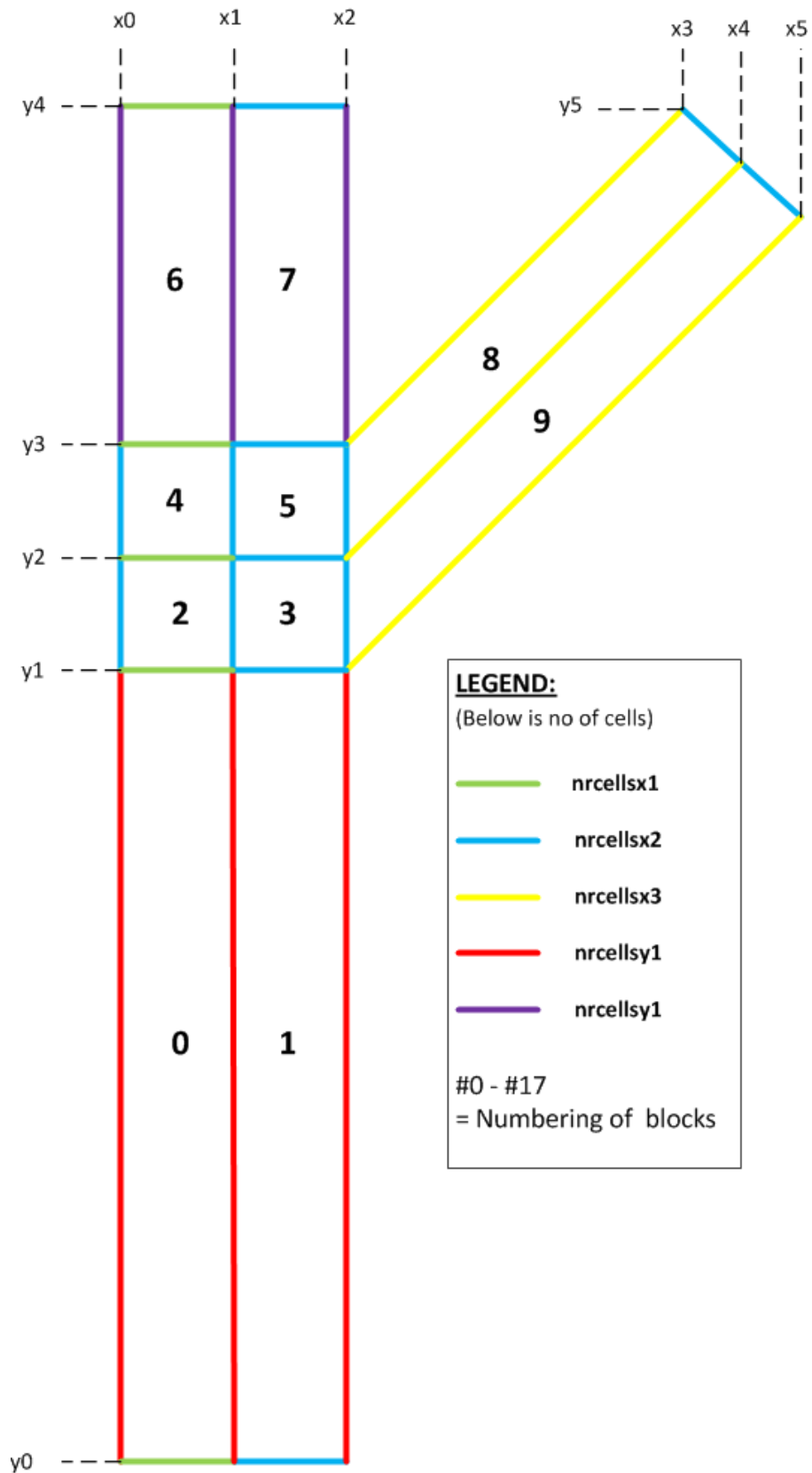
- Hessel, V., Löwe, H., Schönfeld, F., 2005. *Micromixers – a review on passive and active mixing principles*. Chemical Engineering Science 60, 2479-2501
- Henzler, H.J., 1978. *Investigations on mixing fluids*. Dissertation, RWTH Aachen 60.
- Igor Tkatchenko, Nikolai Kornev, Steffen Jahnke, Günter Steffen, Egon Hassel, October 2006, *Performances of LES and RANS Models for Simulation of Complex Flows in a Coaxial Jet Mixer*, Springer Science 2007
- J. Baldyga, J.R. Bourne, 1999, *Turbulent Mixing and Chemical Reactions*, John Wiley & Sons, New York.
- J.H. Ferziger, M.Perić, *Computational Method for Fluid Dynamics*, 3rd Edition, 2002, Springer.
- JurijSODJA, Rudolf Podgornik, March 2007. *Turbulence model in CFD*, University of Ljubljana.
- K.H. Tebel, H.O. May, *The open jet reactor - an effective reactor Design for the suppression of selectivity losses by fast, unwanted side reaction*, Chem Eng. Tech. 60: (11) (1988) 1708-1788
- Kruis, F.E, Falk, L., 1996. *Mixing and reaction in a tubular jet reactor: a comparison of experiments with a model based on a prescribed PDF*. Chemical Engineering Science 51 (10), 2439-2448.
- Launder, B., Reece, G., Rodi, W.: *Progress on the developments of a Reynolds-stress turbulence closure*. J. Fluid Mech. 68, 537-566 (1975)
- Lima, M., Palma, J., 2002. *Mixing in coaxial confined jets of large velocity ratio*. Proceedings of the 10th International Symposium on Application of Laser Technique in Fluid Mechanics, Lisboa, 8-11 July.
- Liu. Y, Fox. R.O., *CFD Predictions for Chemical Processing in a Confined Impinging Jets Reactor*, AIChE Journal, 2006, Vol. 52, 731-744

- Menter, F.: *Zonal two equation k - ω turbulence models for aerodynamics flows*. AIAA-paper 1993-2906, (1993)
- Michael Casey, Torsten Wintergerste, *Best Practice Guidelines, Version 1.0*, Fluid Dynamics Laboratory, January 2000
- Middleton, J.C., Pevice, F., Lymch, P.M., 1986, *Computational of flow fields and complex reaction yield in turbulent stirred reactors and comparison with experimental data*, Chemical Engineering Research and Design 64, 18-21
- Mortensen, M., Orciuch, W., Bouaifi, M., Anderson, B., 2003. *Mixing of a jet in a pipe*. Transactions of Institution of Chemical Engineers 81 (A), 1-7.
- Nere, N.K., Patwardhan, A.W., Joshi, J.B., 2003, *Liquid-phase mixing in stirred vessels: Turbulent flow regime I*, Industrial and Engineering Chemistry Research 42, 2261-2698.
- Paul, E.L., 2003. *Handbook of Industrial Mixing: Science and Practice*. Wiley, New York.
- Pei-Cheng Lou, Yi Cheng, 2007, *Millisecond mixing of two liquids streams in a mixer model*, Chemical Engineering Science 62 (2007) 5688-5695
- R.O. Fox, *Computational Models for Turbulent Reacting Flows*, Cambridge University Press, 2003
- Satoshi Someya, Satoshi Yoshida, May 2009, *The effect of chemical reaction on the mixing flow between aqueous solutions of acetic acid and ammonia*, International Journal of Heat and Mass Transfer 52 (2009) 4236-4243
- Valery Zhdanov, N. Kornev, E. Hassel, A. Chorny, *Mixing of confined coaxial flows*, International Journal of Heat and Mass Transfer 49, 3942-3956 (2006)
- Valery Zhdanov, N.V. Kornev, and E. Hassel, *LIF investigation of the concentration field in the coaxial mixer*. Lasermethoden in der Stroemungsmesstechnik, 12 Fachtung, 7-9 September, 2004. Karlsruhe: Universitaet Karlsruhe, 2004, pp. 16-1-16-8.

- Villermaux, E., Rehalb, H., 2000. *Mixing in coaxial jets*. Journal of Fluid Mechanics 425, 161-185.
- Y. Liu, H. Feng, M.G. Olsen, R.O. Fox, J.C. Hill, *Turbulent mixing in a confined rectangular wake*, Chemical Engineering Science 61 (2006) 6946-6962
- Y.N. Chiu, J. Naser, K.F. Ngian, K.C. Pratt, January 2009, *Computational of the flow and reactive mixing in dual-Rushton ethoxylation reactor*, Chemical Engineering and Processing 48 (2009) 977-987
- Zhe Liu, Yi Cheng, Yong Jin, 2009, *Experimental study of reactive mixing in a mini-scale mixer by laser-induced fluorescence technique*, Chemical Engineering Engineering Journal 150 (2009) 536-543

APPENDIX A: Geometry Description for Fast Mixing Nozzle





In the next pages are a set of codes that have been used in making the geometry. The geometry was created using M4 file. Later on, once the M4 is finished, it will be converted into the original file format (named as blockMeshDict) which is readable by the OpenFOAM to construct the geometry structure.

The structure of the codes can be divided into several sections, such as below:

- Header file (a set of notes which will be not read by the solver)
- Set of definitions (describe all the specifications of the geometry include the length, wide, number of cells and the location of vertices)
- Set of vertices (describe each and every vertices that are used in the geometry)
- Set of blocks (describe the location and size of blocks that is created by joining 8 vertices to form volume of blocks)
- Set of patches (defined the locations and the types of faces that will be used as the boundary condition)

Using M4 file is similar to blockMeshDict file except M4 file can easily define the grid size and it is more flexible in controlling the grid size of the geometry. This M4 file needs to be converted to regular blockMeshDict file so that OpenFOAM can read the geometry of the case. To convert from M4 file to blockMeshDict, execute 'm4 blockMeshDict.m4 > blockMeshDict' in the constant/polyMesh directory. A regular blockMeshDict file will be created in the directory.

Below are some of the good practices to draw geometry on blockMeshDict and also good grading:

- In dividing the geometry into few blocks, make sure all the blocks must have four edges; this is to avoid forming triangular shape which will make sharp edges. A sharp edge is not good because it will results on bad grading.

- Size of mesh must not have very much difference to the adjacent blocks; the difference can only be different maximum of two or three times larger than the adjacent mesh.
- It was suggested to have blocks as less as possible, but please be reminded that good blocks also need to be flexible so that the length and height can be varies. It is important for the usage of further investigation maybe in the future.
- Always have a good note or documentation on whatever problems and solutions that had been found because it can be very useful for other people to learn from it. And also put any reference on anything that was found like an article or references.

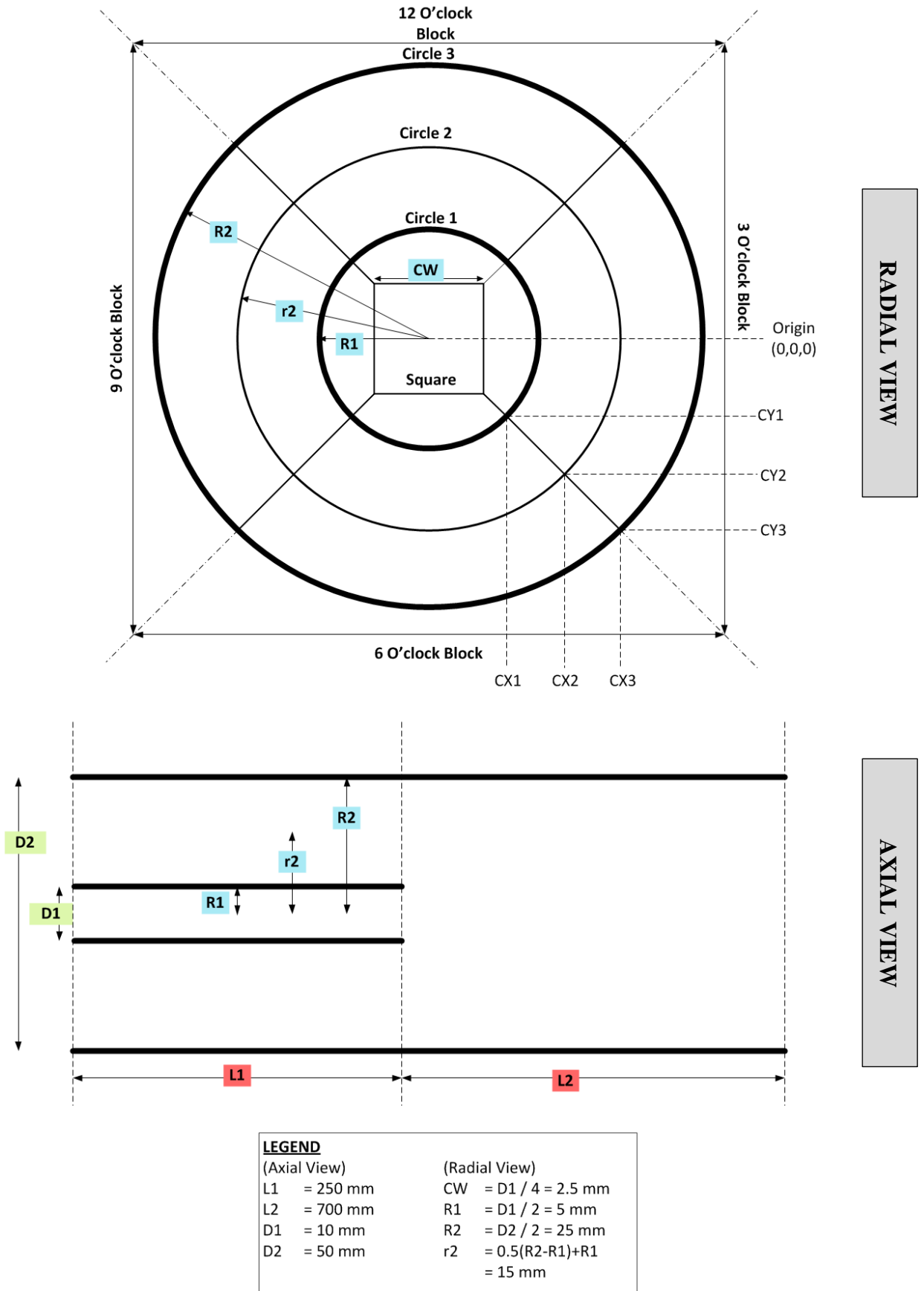
BlockMeshDict. M4

(Geometry Codes in M4 format file)

BlockMeshDict

(Geometry Codes in standard OpenFOAM format
file – after been converted)

APPENDIX B: Geometry Description for Coaxial Mixer Jet



BlockMeshDict. M4

(Geometry Codes in M4 format file)

BlockMeshDict

(Geometry Codes in standard OpenFOAM format
file – after been converted)

B.1 How To ‘Make an Internal Wall’ of the inner pipe of coaxial jet mixer

This tutorial is to describe on how to make an internal wall for blockMeshDict because blockMesh can never accept any boundary in internal face. Basically, the internal wall was created using *createBaffle* utility provided in OpenFOAM installation, but the hardest part was to specify the specific faces needed to make the internal wall. So, this tutorial is meant for a complex geometry. In the first part of this tutorial, a general instruction on using *createBaffle* will be explain. Then, on the second part, details of the steps will be explained with some example using a simple 3-D geometry.

B.2 How To... createBaffle

- 1) First, generate geometry in blockMesh.
- 2) Then, specify the specific area/zone/location/volume needed to make the internal wall.
- 3) Specify the specific faces needed in *constant/polyMesh/sets* directory. (Note: This sets file is important to tell the computer that this location need to make a new boundary)
- 4) Edit the boundary file in *constant/polyMesh* directory by adding a new boundary with zero no. of face (nfaces 0;) and change the new count number on the top of the boundary file.
- 5) Then, return to the main case directory and execute the utility command:
createBaffle <set> <patch>

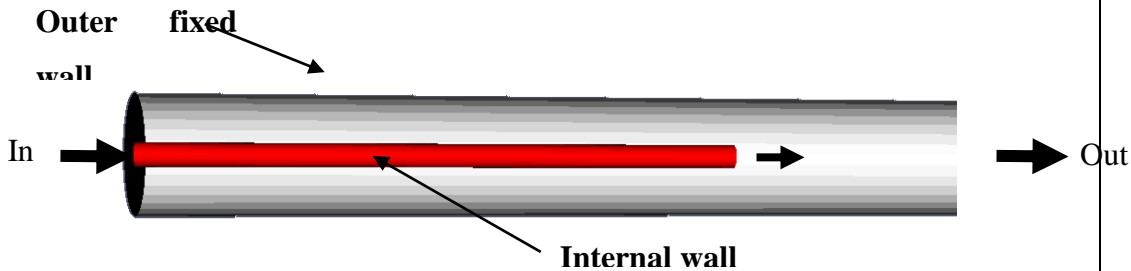
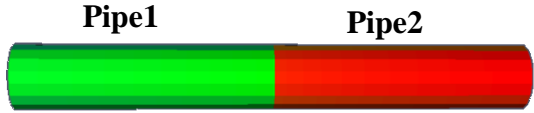
Notes:

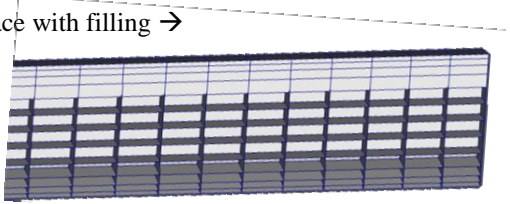
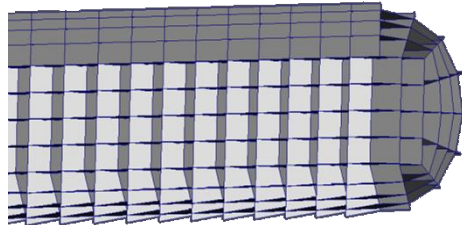
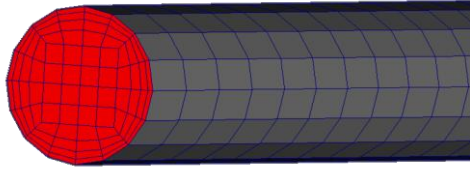
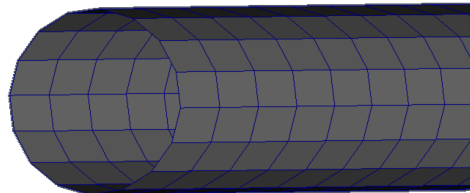
<set> The name of the file in the sets folder that contains the specified faces need to create the internal boundary

<patch> The new boundary name specified in the boundary file

- 6) A new time directory will be created that contains a polyMesh folder.
- 7) Move this polyMesh folder into constant directory, and replace with the old polyMesh folder. (Caution: It is recommended not to replace or delete the old polyMesh file. Just uncommand or rename the old file because maybe it can be useful in the future for reference)

B.3 Details Instruction

Our Aim/Objective		
		
Description	Example	
1.	<ul style="list-style-type: none"> generate blockMesh mark the block which we want to modify, so a cellZones file will be created 	<p>In the blockMeshDict.M4 file :</p> <pre>***** blocks (Hex (a1 b1 c1 d1 a2 b2 c2 d2)pipe1 (1 1 1) simpleGrading(1 1 1) Hex (a1 b1 c1 d1 a2 b2 c2 d2)pipe2 (1 1 1) simpleGrading(1 1 1))</pre>
2.	<ul style="list-style-type: none"> Use command setSet, and a new command will display. Now we have two set of cell in cellZones: <ul style="list-style-type: none"> ✓ Pipe1 = internal pipe inlet ✓ Pipe2 = internal 	 <p>Pipe1 will be the targeted face that is needed, while pipe2 will be deleted later.</p>
3.	<ul style="list-style-type: none"> In the setSet command, type <code>cellSet pipeFace1 new zoneToCell pipe1</code> Do the same with zone pipe2 <code>cellSet pipeFace2 new zoneToCell pipe2</code> 	<p>Note: Here, a new cell set file will be created named '<code>pipeFace1</code>' from the function '<code>zoneToCell</code>' refer to zone '<code>pipe1</code>'</p> <p>Zone '<code>pipe2</code>' → cells '<code>pipeFace2</code>'</p>

<p>4.</p>	<ul style="list-style-type: none"> Now, create faceSet for pipe1 <pre>faceSet <u>facePipe</u> new cellToFace <u>pipeFace1 all</u></pre> <ul style="list-style-type: none"> This conversion from cell to face will change all cells to faces, but the problem is, it will create all faces including the internal/filling of the pipe1, and we don't want this. 	<p>cellSet 'pipeFace1'</p> <p style="text-align: center;">↓ cellToFace</p> <p>faceSet 'facePipe'</p> <p>Face with filling →</p>  <p style="text-align: center;"><i>facePipe</i></p>
<p>5.</p>	<ul style="list-style-type: none"> Eliminate the internal face inside faceSet 'facePipe' Create another faceSet that contained the internal face <pre>faceSet <u>faceFilling</u> new cellToFace <u>pipeFace1 both</u></pre>	<p>The command is still same on making faceSet 'facePipe', but instead of all, we choose both.</p> <p>Both mean choose everything except the boundary layer.</p>  <p style="text-align: center;"><i>faceFilling</i></p>
<p>6.</p>	<ul style="list-style-type: none"> Then, we can remove all the internal faces using function delete. <pre>faceSet <u>facePipe</u> delete faceToFace <u>faceFilling</u></pre> <ul style="list-style-type: none"> Remove the inlet faces <pre>faceSet <u>facePipe</u> delete boundaryToFace</pre>	<p>Before use boundaryToFace:</p>  <p>After removing use boundaryToFace:</p> 

<p>7.</p>	<ul style="list-style-type: none"> • Almost done except the other side of outlet faces. Here, we must remove by using <i>intercept</i> function, by delete all faces that intercept between pipe1 and pipe2. • Create a new faceSet that have the faces of interception between pipe1 and pipe2 <pre>faceSet <u>faceSubset</u> new cellToFace <u>pipeFace2</u> all</pre> <pre>faceSet <u>faceSubset</u> subset faceToFace <u>facePipe</u></pre> <ul style="list-style-type: none"> • Now, remove all the faces that intercept between faceSet 'facePipe' with 'faceSubset' <pre>faceSet <u>facePipe</u> delete faceToFace <u>faceSubset</u></pre> <ul style="list-style-type: none"> • Then, we get the full face that we needed to create internal boundary using createBaffle 	<pre>cellSet 'pipeFace2'</pre> <p style="text-align: center;">↓ cellToFace</p> <pre>faceSet 'faceSubset'</pre> <p style="text-align: center;">↓ faceToFace</p> <pre>faceSet 'faceSubset'</pre> <p>(only face that intercept between faceSubset and facePipe)</p>
<p>8.</p>	<ul style="list-style-type: none"> • The important steps are to edit the boundary file in the <i>constant/polymesh</i> directory. • Add a new boundary name with zero face number (nfaces 0;) and start the face numbers from the last numbering (please add the last number from the previous boundary name with its number of faces) • And don't forget to change the new number of boundary on the top of the file, otherwise you will receive an error message. <p>(NOTE : If you have probe function in the controlDict file, please disable it because they will give an error message when you run splitMesh or createBaffles)</p>	<p>Example of new boundary in boundary file:</p> <pre>***** internalWall { type wall; nFaces ; //(just zero) startFace 1528128; } *****</pre>

9.	<ul style="list-style-type: none"> • Then, proceed with the splitting or creating baffle. (Refer instruction on how to use <i>createBaffle</i> utility) 	
----	--	--

~.setSet (a batch file)



```
// Create a cell set from zone pipe1 and pipe2
cellSet pipeFace1 new zoneToCell pipe1
cellSet pipeFace2 new zoneToCell pipe2

//Create a face set from cellSet of pipeFace1
faceSet facePipe new cellToFace pipeFace1 all

//Create a set of all faces except at the outside faces (boundary
wall)
faceSet faceFilling new cellToFace pipeFace1 both

//remove all internal faces inside the pipe and at the inlet(a.k.a
inletSmall) of the pipe
faceSet facePipe delete faceToFace faceFilling
faceSet facePipe delete boundaryToFace

//Create a set of faces that intercept between pipe1 & pipe2
faceSet faceSubset new cellToFace pipeFace2 all
faceSet faceSubset subset faceToFace facePipe

//Remove the outlet faces of the pipe that intercept with pipe2
faceSet facePipe delete faceToFace faceSubset

quit
```



How to run:

setSet -batch <name of the set script> to run a setSet script file

(example: setSet -bash .setSet)

APPENDIX C: Case Setup

C.1 K- ϵ model

- 1) First, after finish generating the mesh with `m4`, export it into `blockMeshDict` file and define the boundary conditions in the time folder. K- ϵ model was used as the first initial model. Therefore, uniform value was defined in the initial boundary conditions.
- 2) Check the mesh with `checkMesh` utilities by typing '`checkMesh`'.
- 3) Edit the physical properties in `constant/transportProperties` with kinematic viscosity, `nu` and fluid density, `rho` in SI units.
- 4) Edit `constant/RASproperties` to specify the type of turbulence model; in this case, `kEpsilon` model was used.
- 5) Edit all boundary files in the `0` directory (*zero-time-folder*) to match the physical boundary file.
- 6) Edit all solver's settings in `system` folder. For example; `controlDict` file for solution steering (i.e `startTime`, `endTime`, `DeltaT`, `writeInterval` & etc)
- 7) Run the solver ; `simpleFoam > log&` ('log' means to write the residual in a new file named 'log')

C.2 RNG and realizable k- ϵ model

- 1) The previous initial case of k- ϵ model was copied with the latest time folder. Or, it can also be done by using field mapping utility. This utilities required `mapFieldsDict` file in the `system` directory. This utilities was run by typed '`mapfields <source file> -sourceTime <time>`'.

Example: `-mapFields ../mesh1kepsilon -sourceTime 1000`

(This mean, mapping from `kEpsilon` model in `mesh1kepsilon` at time 1000)

- 2) Edit `constant/RASproperties` to change the turbulence model
- 3) Run the solver with log file to observe the final residual results.
(`simpleFoam > log&`)

C.3 Finer mesh with smaller grid size

- 1) The previous coarser-mesh case was copied to other folder and it is recommended to copy from the same type of turbulence model.

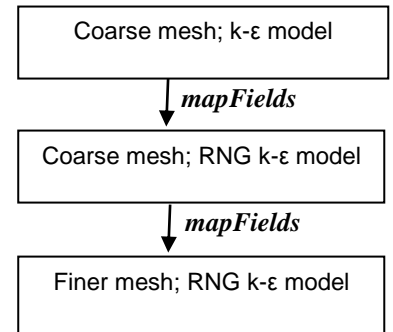
(Example: copy *mesh1realizable* → *mesh2realizable*)

- 2) The number of cells was increased by editing the geometry definition in m4 file, with factor of 2 in every direction. Then, export it into readable *blockMeshDict*;

(i.e *blockMeshDict.m4* > *blockMeshDict*)

- 3) The boundary condition's fields were mapped using *mapFields* by taking the coarser mesh as a mapping source. Figure X shows the strategy of mapping fields.

- 4) Run the solver as usual.

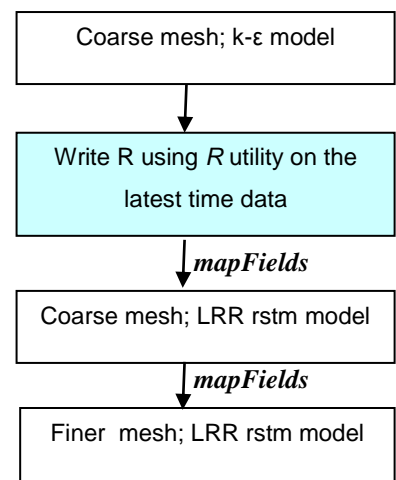


C.4 LRR and Launder Gibson RSTM model

- 1) For this kind of turbulence model, a new variable needed which is *Reynold Stress Tensor; R*. It was important to have *nonuniform* boundary conditions; otherwise the solution will not converge even until a lot of iterations. k-ε model was used as a mapping source and it is recommended to map from the source that had a same grid size of mesh.

- 2) Before do mappings, use *R* utility to create the Reynold Stress Tensor in the boundary condition file of a mapping source latest time file. This utility will write the value of *R* depend from the other variables like *U*, *k* and *epsilon*.

- 3) Run the solver as usual. Figure X shows the strategy on running for RSTM model simulation.



C.5 k- σ model

- 1) For kOmega model, all the case setup was still the same as RSTM model but it needs one more variable which called *omega*, and this variable was not necessary to have a nonuniform boundary condition.
- 2) The different with the other model was this model will not calculate for *turbulence dissipation energy*, ε . Therefore, *writeEpsilon** utility was used to calculate the value of ε at latest time folder. With this, we can use the value ε as a comparison with other model or other grid size.

(Example: `writeEpsilon -latestTime`)

* *writeEpsilon* utility was created new. It does not come with the default OpenFOAM installation.

APPENDIX D: Post-Processing

D.1 Graph Plotting using *gnuplot* version 4.2

During the post processing step, I use *gnuplot* to plot the data gathered using `sampleDict` command which will explain in the next paragraph. Below is the example of *gnu* file command that I used in this case.

Command	Description
<code>set terminal png giant transparent</code>	The terminal was set to have <i>png</i> file format for the output, in giant size graph, transparent background and by default, it will plot with colour line
<code>set output "10mm.png"</code>	The output will be named as <i>10mm.png</i>
<code>set multiplot</code>	To have more than one plot in one graph
<code>set key bottom title 'Legend'</code>	This command is to create a graph's legend with title name of 'Legend', located at the bottom of the graph
<code>set autoscale</code> <code>set xlabel "Iteration Time"</code> <code>set ylabel "Magnitude"</code>	This plot will scale up automatically with a suitable scale. The X-axis was named as ' <i>Iteration Time</i> ' and for the Y-axis was named as ' <i>Magnitude</i> '
<code>set xtics 0,0.1,0.5</code>	<i>xtics</i> should be define if the user want to set the x-axis interval manually. <i>0,0.1,0.5</i> mean that the x-axis start from <i>0</i> , with each interval had a <i>0.1</i> different, until <i>0.5</i>
<code>set ytics 0.2</code>	Same as <i>xtics</i> but here is to the y-axis with interval of 0.2 each
<code>set title "Line plot of different meshes at y=10mm"</code>	The title of the graph was named as 'Line plot of different meshes at y=10mm'
<code>plot "LG2y_10mm_Tracer.xy" using 1:2</code> <code>title "Experimental" w point</code>	This command tells <i>gnuplot</i> to take data from file named 'LG2y_10mm_Tracer.xy' and <i>using 1:2</i> represent the column X:Y, with title of 'Experimental' and plot <i>with point</i> Other option of <i>with</i> are : lines, points, linespoints, impulses, dots, steps, fsteps, histeps, errorbars, xerrorbars, yerrorbars, xyerrorbars, boxes, boxerrorbars, boxxyerrorbars, financebars, candlesticks or vector
<code>set nomultiplot</code>	To reset the <i>gnuplot</i> back to non-multiplot function

Below is the example of *gnuplot* file format.

```
1
2 set terminal png giant transparent
3 set output "10mm.png"
4 set multiplot
5 set autoscale
6 set xrange [0:2]
7 set yrange [-0.1:1.1]
8 set key bottom title 'Legend' #below
9
10 set xlabel "x, mm"
11 set ylabel "Normalized concentration of liquid B"
12 set title "Line plot of different meshes at y=10mm"
13 set xtics 0,0.1,0.5
14 set ytics 0.2
15
16 plot "LG2y_10mm_Tracer.xy" using ($1*1000):4 title "LG RSTM" w l,
17 "phy4_y10.txt" using 1:2 title "Experimental" w point
18
19 set nomultiplot
20 reset
```

D.2 Viewing the grid size and contour using *Paraview Ver 3.6.2*

